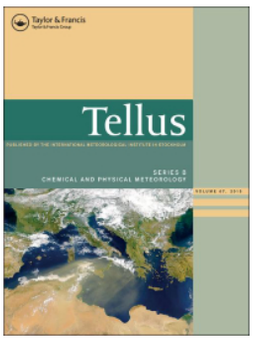

Tellus B: Chemical and Physical Meteorology

ISSN: (Print) (Online) Journal homepage: https://www.tandfonline.com/loi/zelb20

# Analysis of the temporal variability of $CO_2$, $CH_4$ and CO concentrations at Lamto, West Africa

**Toure Dro Tiemoko, Michel Ramonet, Fidele Yoroba, Kobenan Benjamin Kouassi, Kouakou Kouadio, Victor Kazan, Claire Kaiser, François Truong, Cyrille Vuillemin, Marc Delmotte, Benoit Wastine & Phillipe Ciais**

**To cite this article:** Toure Dro Tiemoko, Michel Ramonet, Fidele Yoroba, Kobenan Benjamin Kouassi, Kouakou Kouadio, Victor Kazan, Claire Kaiser, François Truong, Cyrille Vuillemin, Marc Delmotte, Benoit Wastine & Phillipe Ciais (2021) Analysis of the temporal variability of $CO_2$, $CH_4$ and CO concentrations at Lamto, West Africa, Tellus B: Chemical and Physical Meteorology, 73:1, 1-24, DOI: 10.1080/16000889.2020.1863707

**To link to this article:** https://doi.org/10.1080/16000889.2020.1863707



Published online: 26 Dec 2020.

Tellus SERIES B CHEMICAL AND PHYSICAL METEOROLOGY
PUBLISHED BY THE INTERNATIONAL METEOROLOGICAL INSTITUTE IN STOCKHOLM



# Analysis of the temporal variability of $CO_2$, $CH_4$ and CO concentrations at Lamto, West Africa

*By* TOURE DRO TIEMOKO[1]*, MICHEL RAMONET[2], FIDELE YOROBA[1,3], KOBENAN BENJAMIN KOUASSI[1,3], KOUAKOU KOUADIO[1,3], VICTOR KAZAN[2], CLAIRE KAISER[2], FRANÇOIS TRUONG[2], CYRILLE VUILLEMIN[4], MARC DELMOTTE[2], BENOIT WASTINE[2], and PHILLIPE CIAIS[2], [1]*UFR SSMT, Laboratory of Atmosphere Physic and Mechanic Fluids (LAPA-MF), University Felix Houphouet-Boigny, Abidjan, Côte d'Ivoire;* [2]*Laboratoire des Sciences du Climat et de l'Environnement (LSCE), IPSL, CEA-CNRS-UVSQ, Université Paris-Saclay, Gif-sur-Yvette, France;* [3]*Geophysical Station of Lamto (GSL), N'Douci, Côte d'Ivoire;* [4]*CEA/IRFU/DEDIP, France*

(Manuscript Received 1 July 2020; in final form 10 December 2020)

ABSTRACT

The 10-year observations of the atmospheric molar fractions of $CO_2$, $CH_4$ and CO in West Africa were analyzed using a high precision measurement of the Lamto (LTO) station (6°31 N and 5°02 W) in Côte d'Ivoire. At daily scale, high concentrations appear at night with significant peaks around 7 a.m. local time and minimum concentrations in the afternoon for $CO_2$ and $CH_4$. The CO concentrations show two peaks around 8 h and 20 h corresponding to the maximum in road traffic of a northern motorway located 14 km from the station. The long-term increase rates of $CH_4$ (~7 ppb year$^{-1}$) and $CO_2$ (~2.24 ppm year$^{-1}$) at Lamto are very close to global trends. The variations of the concentrations of the three gases show strong seasonality with a peak in January for all gases and minima in September for $CO_2$ and $CH_4$, and in June for CO. The CO variation suggests a significant impact of fires on the CO, $CO_2$ and $CH_4$ anomalies in the Lamto region during the dry season (December to February). CO and $CH_4$ show strong correlations (at synoptic-scale and monthly based) in January ($r = 0.84$), February ($r = 0.90$), April ($r = 0.74$), November ($r = 0.79$) and December ($r = 0.72$) reflecting similar sources of emission for both gases. The trajectories of polluted air masses at LTO, also indicate continental sources of emission associated with Harmattan winds.

*Keywords: greenhouse gases, carbon dioxide, methane, carbon monoxide, Lamto*

## 1. Introduction

The impact of climate change in Africa is projected to be adverse for ecosystems and water resources (GIEC, 2014) and could undermine socio-economic and health stability. Also, of the ten most threatened countries by climate change in the world, seven are African (i.e. Central African Republic, Eritrea, Ethiopia, South Sudan, Chad, Nigeria and Sierra Leone). Furthermore, the sub-Saharan West African region is subject to a fast population increase (>3% year$^{-1}$) (UNDP, 2015; Ago et al., 2016) and land-use change with cropland expansion over natural ecosystems. In addition, the FAO report of 2011 (FAO, 2011) highlighted reducing areas of wetlands and forests, with a 1.1% year$^{-1}$ average forest cover loss during the 2000-2010 period, with important losses of –5.1% year$^{-1}$ for Togo, –3.7% year$^{-1}$ for Nigeria and –2.1% year$^{-1}$ for Ghana. In the same vein, the regional temperature increased by 0.2 to 0.8 °C in West Africa since the late 1970s (CEDEAO-CSAO/OCDE, 2008). Also, West Africa has experienced decrease by 40% to 60% in the annual average flow of the major rivers (Niasse, 2004). This region experienced extreme heat events and heat waves such as those observed in Niger in 2010 (Ringard et al., 2014; Karimou et al., 2015) causing deaths among vulnerable populations. Africa has been exposed to more than 136 drought episodes in the 1995–2015 period of which 77 (i.e. 56.61%) for the East African region alone (https://www.afdb.org/en/cop23/

*Corresponding author. email: ttouredro017@gmail.com





Citation: Tellus B: 2021, **73**, 1863707, https://doi.org/10.1080/16000889.2020.1863707

cop23-overview/). The region is also a hotspot of fire activity, accounting for more than 50% of global fire emissions (van der Werf et al., 2010; Scholes et al., 2011) although a reduction of burned areas (Andela and van der Werf, 2014) and emissions are observed from satellite data since the year 2000, related to rainfall increase and cropland area expansion.

Although it is widely recognized that African ecosystems play a major role in the carbon cycle, uncertainties remain very important in both the mean magnitude of carbon fluxes and their inter-annual variability (Bombelli et al., 2009). Few long-term carbon cycle observations are available in Africa, particularly in West Africa, with five eddy covariance towers (Merbold et al., 2009) and up to this study, no atmospheric station. As a result of atmospheric data scarcity, the results from atmospheric inversions used to infer the distribution of sources and sinks at the surface from atmospheric concentration observations and atmospheric transport models (Ciais et al., 2010) have large uncertainties across the region. Chevallier et al. (2014) attributed natural (fossil fuel removed) $CO_2$ emissions to North Africa, ranging from 0.5 to more than 1 GtC $yr^{-1}$ depending if they use surface in-situ or satellite data (GOSAT). More recently the major role of northern tropical Africa in the $CO_2$ budget has been confirmed with an emission estimated to about 1.5 GtC $yr^{-1}$ (Palmer et al., 2019) based on the inversion of $CO_2$ total column retrieved from GOSAT and OCO-2 satellites. The scarcity of ground-based measurements constitutes a hindrance to provide robust estimates of $CO_2$ sources and sinks in this region (Palmer et al., 2019). Moreover, the estimation based on satellite inversions are sensitive to the aerosol bias in the retrieval of column $CO_2$ and to transport uncertainty.

In the present study, we present the longest in situ time series of $CO_2$ and $CH_4$ concentrations monitored in West Africa, from the Lamto station (LTO), located in the wet tropical region of West Africa in Côte d'Ivoire. The observatory of Lamto was setup in 2008 as part of the CARBOAFRICA European project (www.carboafrica.eu). The main use of this type of data is to feed global to regional inversion studies. This paper presents a synthesis of the seasonal and diurnal cycles of greenhouse gases recorded over the 10 years (2008–2018). Besides, we present a record of carbon monoxide from the station, CO being a key pollutant and a surrogate tracer that can detect combustion processes (Turnbull et al., 2006; Wang et al., 2010; Duren and Miller, 2012). The concentration of $CO_2$, $CH_4$, and CO continuously measured from the Lamto station are compared with flask air samples from three stations located in the Sahara Desert (Assekrem, ASK), in the Canarias Is. (Izana, IZO) and the tropical Atlantic Ocean (Ascension Island, ASC) as part of the National Oceanic and Atmospheric Administration (NOAA-ESRL) global air sampling network and to the continuous measurements of the Cape Verde Atmospheric Observatory (CVO) (Kozlova and Manning, 2009) to highlight significant trends of the greenhouse gases concentrations variations. This work is structured as follows; Section 2 describes the study area, the material, and the method used. Section 3 shows the results of the $CO_2$, $CH_4$ and CO atmospheric records. Conclusions and perspectives are given the last section.

## 2. Study area, material, and methods

### 2.1. Study area

The Lamto station (6°31 N and 5°02 W) is located within a 2700 ha nature reserve, about 160 km north of Abidjan, at an altitude of 155 m above the sea level (Fig. 1) in a flat region without striking relief. The surrounding vegetation is a wet tropical savanna, in the transition area between forest and savanna (Diawara et al., 2014). The Taabo hydroelectric dam, built on the Bandama River, is located 6 km east of the station (Kouassi et al., 2008). Long times series measurements of climate data (i.e. temperature, rainfall, relative humidity, wind speeds and direction, radiative heat, etc.) have been carried out at the Geophysical station since 1962 (Abbadie et al., 2006; Diawara et al., 2014). In addition, the mean annual rainfall and temperature records are at 1194 mm and 27.8 °C, respectively (Diawara et al., 2014; N'dri et al., 2018). The climate of this area is controlled by the West African Monsoon (WAM) with the main dry season (GSS) from December to February, the main rainy season (GSP) from March to July, a short dry season (PSS) in August and a short rainy season from September to November (Fig. 2). On the other hand, the anthropogenic activities around the station are mainly related to agriculture, fishing and livestock. Also, the A3 highway connecting Abidjan to Yamoussoukro, which records a very dense road-traffic during the day, is located 14 km west of the station. Seasonal bush fires (from December to February) affect more than 80% of the ground biomass (Nacro, 2003).

Furthermore, Fig. 3 shows the average influence functions from surface fluxes given short and medium range transport of air masses to LTO during the main dry (Fig. 3a) and wet (Fig. 3b) seasons. We observe that during the main dry season (GSS), Lamto region is permanently influenced by air masses originating from the northern and north-eastern sectors (Tiemoko et al., 2020b). The presence of these air masses from the northern and north-eastern sectors is related to the harmattan flow regime in the region. However, in the main wet season


Fig. 1. Localisationn of the ASC, ASK, IZO monitoring stations from the NOAA network and from the Lamto reserve (6°31 N et 5°02 W). Picture on the right was taken from the top of the sampling tower (Adapted from Tiemoko et al., 2020b).

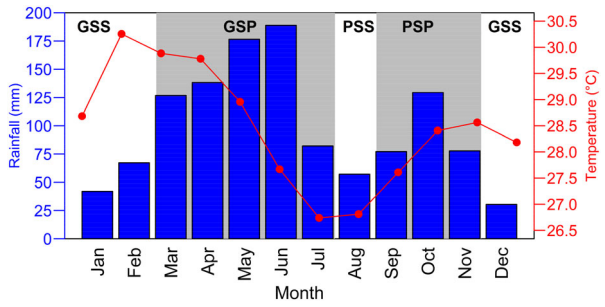


*Fig. 2.* Monthly means of Air Temperature in °C (red) and rainfall in mm (blue) at Lamto over the period 2008–2018. GSS, GSP, PSS and PSP are the great dry season, the great wet season, the short dry season and the short-wet season, respectively.

(i.e. from May to July), the air masses arriving at Lamto are preferentially observed from a tropical Atlantic Ocean and Guinean Gulf coast origin in the south and south-west sectors which are characteristic of the west African monsoon flow.

## 2.2. Atmospheric measurements

*2.2.1. Continuous $CO_2$, $CH_4$, CO measurements at Lamto.* The $CO_2$ and $CH_4$ mole fractions are continuously measured at Lamto station (LTO) since August 2008, and CO measurements started in March 2014. The measurements were obtained using two versions of cavity ring down spectroscopy instruments (CRDS_Picarro_Envirosens and CRDS_Picarro_2401). The Envirosens model (SN: CFADS-02) was used from August 2008 to late 2013 for $CO_2/CH_4/H_2O$ measurements while the G2401 model (SN: 1703-CFKADS-2124) is used since April 2014 for $CO_2/CH_4/H_2O$/CO measurements. These instruments based on cavity ring-down spectroscopy have linear and stable responses, and are recognized for their high accuracy in $CO_2$, $CH_4$ and CO molar fractions measurements (Crosson, 2008; Chen et al., 2010; Yver Kwok et al., 2015). Lamto measurements data are calibrated to the World Meteorological Organization (WMO) reference scales using four calibration gases spanning the atmospheric ranges of concentrations (Table A1). Those tanks are themselves calibrated at LSCE using six calibration tanks from NOAA/ESRL. The air is sampled continuously at the top of a 50 m tower and passes through 2 µm filters to protect the pump and the analyzer from dusts and combustion aerosol (see Fig. 4 and Fig. A1). Since January 2010 a Nafion dryer is used to reduce the amount of water inside the instrument and to minimize the water vapor correction (Rella et al., 2013). In addition to the calibration gases, we measured 2 to 3 times per day a target gas used as a quality control of the measurements. Since 2014 a second target gas was measured at each calibration sequence once or twice a month. This additional target gas (long term target) allows to monitor the measurement reproducibility on longer term periods. This reproducibility over the 10 years period gives a mean bias of $-0.02 \pm 0.04$ ppm for $CO_2$ and $-0.01 \pm 0.17$ ppb for $CH_4$ for target gas values with no significant trend (Table 1), compliant with the recommendations of WMO (Conil et al., 2019), within ±0.1 ppm for $CO_2$ and ±2 ppb for $CH_4$. On the other hand, in the case of CO, we found a mean bias of –6.58 ppb, and a total drift of 2.00 ppb over 4 years, that can be attributed to a drift of the target gas cylinder, or in one of the cylinders used for regular calibration. In order to investigate this problem, new cylinders will be sent to the station to verify the consistency of the calibration scale. Until then, we did not apply any corrections to the CO measurements presented here. We consider that this problem has a low impact on diurnal, synoptic and seasonal

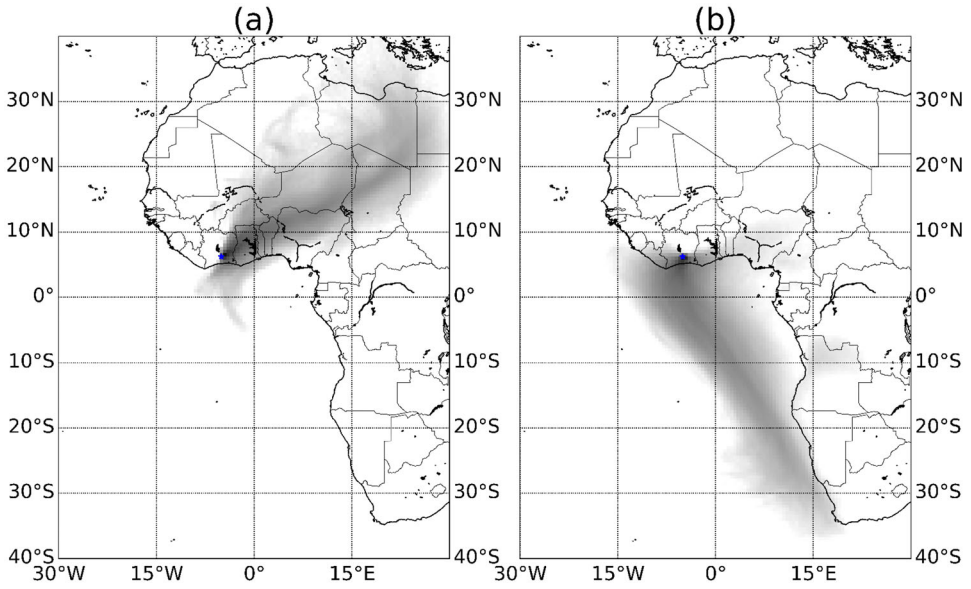


*Fig. 3.* Average retro-plumes of air masses arriving at the station of LTO in the main dry (a) and wet (b) seasons during the 2014–2017 period. In blue, the LTO station.

*Fig. 4.* View of the 50 m high tower. Meteorological sensors are installed at the top of the tower, together with the air intake.

variations. However, we did not analyse the long-term trend and the growth rates of CO in view of calibration cylinders drift.

Maintaining high precision continuous measurements of $CO_2$ and $CH_4$ in a remote site like Lamto is a technical and logistical challenge. With the first CRDS analyser we several problems (one per year on average) leading to data gaps larger than one month. Since the installation of the new analyser in April 2014, we had only one three (3) weeks data gap due to a lightning strike at the station. The regular maintenances of the analyser and different parts of the measurement system are performed by the technical staff of the Geophysical Station of Lamto, under the supervision of LSCE engineers who visit the station once a year on average. The major data gaps can be recalled as follows:

- 04-10-2008 to 22-10-2008: unidentified problem with the analyzer
- 12-05-2009 to 04-07-2009: unidentified problem with the analyzer
- 17-01-2010 to 04-03-2010: crash of the computer (the timestamp no longer works), replaced in March 2010.
- 12-11-2010 to 30-08-2011: breakdown of the analyser due to a problem with the regulation of the warm chamber. Analyzer ESP1000 sent back to the manufacturer in the USA.
- 24-07-2012 to 04-09-2012: stopping the measurements following numerous interruptions of the Picarro analyzer (since the end of May 2012). A new computer was installed.
- 01-09-2013 to 07-04-2014: breakdown of the analyser which cannot regulate the temperature of the cavity.

*Table 1.* Bias and standard deviation calculated for $CO_2$ and $CH_4$ (2008–2018) and CO (2014–2018) during the quality control process at LTO station.

| Gas | Analyzer ID | Cylinder ID | Begin | End | Bias (ppm) | Standard deviation (ppm) |
|---|---|---|---|---|---|---|
| | 23 | D489463 | 28-08-2008 | 29-03-2009 | –0.010 | 0.015 |
| | 23 | D655679 | 30-03-2009 | 05-04-2010 | 0.004 | 0.110 |
| | 23 | D893449 | 05-04-2010 | 12-11-2010 | 0.002 | 0.045 |
| $CO_2$ | 23 | D489463 | 20-11-2011 | 10-05-2012 | –0.003 | 0.015 |
| | 23 | D655679 | 10-05-2012 | 31-05-2013 | –0.0005 | 0.111 |
| | 23 | D856133 | 31-05-2013 | 16-09-2013 | –0.191 | 0.019 |
| | 192 | D893449 | 31-03-2014 | Logs | –0.0005 | 0.015 |
| | 23 | D489463 | 28-08-2008 | 29-03-2009 | –0.002 | 0.103 |
| | 23 | D655679 | 30-03-2009 | 05-04-2010 | 0.034 | 0.193 |
| | 23 | D893449 | 05-04-2010 | 12-11-2010 | 0.021 | 0.360 |
| $CH_4$ | 23 | D489463 | 20-11-2011 | 10-05-2012 | –0.010 | 0.132 |
| | 23 | D655679 | 10-05-2012 | 31-05-2013 | –0.070 | 0.193 |
| | 23 | D856133 | 31-05-2013 | 16-09-2013 | 0.107 | 0.050 |
| | 192 | D893449 | 31-03-2014 | Logs | –0.016 | 0.200 |
| CO | 192 | D893449 | 31-03-2014 | Logs | –6.578 | 2.001 |

Table 2. Reference of the NOAA (ASC, ASK, IZO) and LTO stations for $CO_2$, $CH_4$ and CO concentration measurements.

| Stations | Latitude | Longitude | Altitude (m) | Air intake level (m) |
|---|---|---|---|---|
| ASC (Ascension Island) | 7°57′36′′ S | 14°24′00′′ W | 85 | 3 |
| ASK (Assekrem) | 23°15′36′′ N | 5°37′48′′ E | 2710 | 5 |
| IZO (Izana) | 28°18′00′′N | 16°28′48′′ W | 2372.90 | 5 |
| LTO (Lamto) | 6°13′28′′ N | 5°01′40′′ W | 155 | 50 |
| CVO (Cape Verde) | 16° 51′49 N | 24° 52′02 W | 31 | 30 |

New CRDS analyser set up on 07 April 2014. At the same time a weather station is installed in the vicinity of the air inlet.

- 25-05-2017 to 15-06-2017: lightning of the station. The analyser is safe, but not the computer, time server, and power converter. A maintenance mission is organized in mid-June to replace the damaged parts.

*2.2.2. Regional data from ASC, ASK, IZO and CVO stations.* The closest measurements of $CO_2$ and $CH_4$ are performed on a weekly basis by NOAA/ESRL as part of their cooperative air sampling network (www.esrl.noaa.gov/gmd/ccgg/flask.php) at Assekrem, Algeria (ASK); Ascension Island (ASC) and Izana, Canary Islands (IZO). In situ measurements are also performed at the Cape Verde Atmospheric Observatory (CVO) and retrieved from the WDCGG database (Kozlova and Manning, 2009) (see Table 2). These stations are the closest to LTO in the global network (Fig. 1), at distances of 1900 to 2700 kilometers from LTO. The air flask samples are taken twice a week between 11 h and 16 h (sampling by glass flask) and then analysed at the NOAA/ESRL/GMD laboratory in Boulder, Colorado for the three NOAA stations. The data for $CO_2$, $CH_4$ and CO concentrations are available since 1996 (ASK), 1997 (ASC), 1992 (IZO), and 2012 (CVO), respectively.

### 2.3. Methods

To characterize the long-term trend, seasonal cycle and short-term variations of $CO_2$ and $CH_4$ over the 2008-2018 period, we proceeded by filtering the data measured at LTO, CVO, and at the three nearby NOAA stations (ASC, ASK and IZO). The HYSPLIT (Stein et al., 2015) and FLEXPART (Stohl et al., 2005) models were used to calculate air mass trajectories associated with significant peaks of $CH_4$ and CO concentrations observed in December 2014 during the peak of the fire season.

*2.3.1. Calculating the trend and seasonal cycles.* The curve fitting and data filtering routine (CCGvu) developed by NOAA/CMDL (Thoning et al., 1989) was used

to calculate short-term variations, growth rates, and the average seasonal cycle of $CO_2$, $CH_4$ and CO. For this purpose, the time series of mid-afternoon averages $X(t)$ of each gas (i.e. $CO_2$ ($t$), $CH_4$ ($t$) and CO ($t$)) is decomposed into an adjustment function $f(t)$ and into a residual function $R(t)$ (Equation (1)). The function $f$(t) (Equation (2)) includes a 2-degree polynomial $p(t)$ representing the long term trend and a series of four harmonics that fit the seasonal cycle (Levin et al., 2002; Ramonet et al., 2002; Fang et al., 2017). The residual function $R(t)$ that represents the synoptic variations, obtained by the difference between the hourly mean measurements and the fitted curve $f(t)$ (Lin et al., 2015).

$$X\ (t)\ =\ f(t)\ +\ R(t) \tag{1}$$

$$f\ (t) = p(t) + \sum_{k=1}^{4} \left[a_{2k+1} \sin(2k\pi t) + a_{2k+2} \cos(2k\pi t)\right] \tag{2}$$

where, $p(t) = a_0 + a_1 t + a_2 t^2$, $t$ is the time and the terms $a_i$ are coefficients determined by the least square's method. A combination of high-pass and low-pass filters is applied to $R(t)$ with two respective cut-off frequencies at 80 and 667 days to determine the smoothed time series $S(t)$ (Equation (3)) and long-term trends $T(t)$ (Equation (4)) (Bakwin et al., 1998) . The seasonal cycle Sc($t$) (Equation (5)) is finally obtained by the difference between the smoothed time series $S(t)$ and the long-term trends $T(t)$.

$$S(t)\ =\ f(t)\ +\ R^{80}(t) \tag{3}$$

$$T(t)\ =\ p(t)\ +\ R^{667}(\mathrm{t}) \tag{4}$$

$$Sc(t)\ =\ S(t)\ -\ T(t) \tag{5}$$

*2.3.2. Calculating of trend by Liebmann's method.* An analysis of long and short-term trends in $CO_2$ and $CH_4$ is provided using a statistical diagnosis based on linear regression by least square fit (Liebmann et al., 2010). Trends are calculated by multiplying the slope of linear trends by the length of the time-serie. The most significant trends are obtained with a 95% confidence level by the Student t-test. This method shows robust and specific performances to objectively determine one or more trend breaks in time-series when they occur. In addition, it has been used in many studies on climate variability in West Africa (Diawara et al., 2014; Ta et al., 2016; Tiemoko et al., 2020a).

*2.3.3. Computing of species ratios.* The computing of concentrations ratios allows diagnosing co-variations between the different gases (i.e. $CO_2$, $CH_4$ and CO). Hourly residual time series (i.e. $\Delta CO_2$, $\Delta CH_4$ and $\Delta$CO) were calculated by the difference between the raw data and the smoothed time series described above. These residual time series represent synoptic-scale variations (Harris et al., 2000; Ramonet et al., 2002; Grant et al., 2010; Tohjima et al., 2014; Lin et al., 2015). Concentration ratios of residuals ($\Delta CO_2/\Delta CH_4$, $\Delta CO_2/\Delta$CO and $\Delta CH_4/\Delta$CO) are finally calculated from the regression slope between residual anomalies of different gases, using the Deming regression method (Guérette et al., 2018; Wu and Yu, 2018).

## 3. Results and discussions

### *3.1. Time series analysis and general statistics*

Figure 5a–c shows the time series of the hourly $CO_2$, $CH_4$ and CO atmospheric concentrations. In blue are represented daytime observations from 11 h am to 17 h local time. The choice of separating night and day is based on the variations of the ABL (Atmospheric Boundary Layer) diurnal cycle. The ABL is practically in a stable state during the night (not very turbulent) while it is most often unstable (turbulent) during the day (Fernández-Duque et al., 2017; Mai et al., 2020) resulting in different vertical dilution of local fluxes and influence from more remote fluxes.

The diurnal variations of $CO_2$ and $CH_4$ are characterized by lower concentrations during the day (i.e. 11 h to 17 h) and by higher concentrations during the night (17 h of the day $j$ to 11 h of the day $j+1$), mainly due to ABL development, which dilutes $CO_2$ and $CH_4$ exchanged at the surface and decreases their values during the morning (Murayama et al., 2003; Marnas, 2009). The relative diurnal $CO_2$ variations are more pronounced than those of $CH_4$ due to the covariance of photosynthesis and respiration and ABL depth. The existence of a diurnal cycle of $CH_4$ also suggests $CH_4$ sources in the surroundings of the station, especially for the night time footprint. One possibility for this local $CH_4$ emission corresponds to the Taabo dam take it off located 6 km from the station. The $CO_2$ and $CH_4$ time series also show clear upward trends over the studied period, which are discussed in the section about the growth rates. During the observation period, 29% of the $CO_2$ values are less than 395 ppm, 64% between 395 and 420 ppm and 7% are higher than 420 ppm. For $CH_4$, about 8% of the data below 1800 ppb, 74% are between 1800 and 1900 ppb and only 18% are greater than 1900 ppb. This statistic shows that more than 50% of $CO_2$ and $CH_4$ observations are higher than reported at several monitoring stations listed by the WDCGG (World Data Centre for Greenhouse Gases) Data Summary No. 41. (WMO, 2017), indicating the significant impact of anthropogenic activities and natural

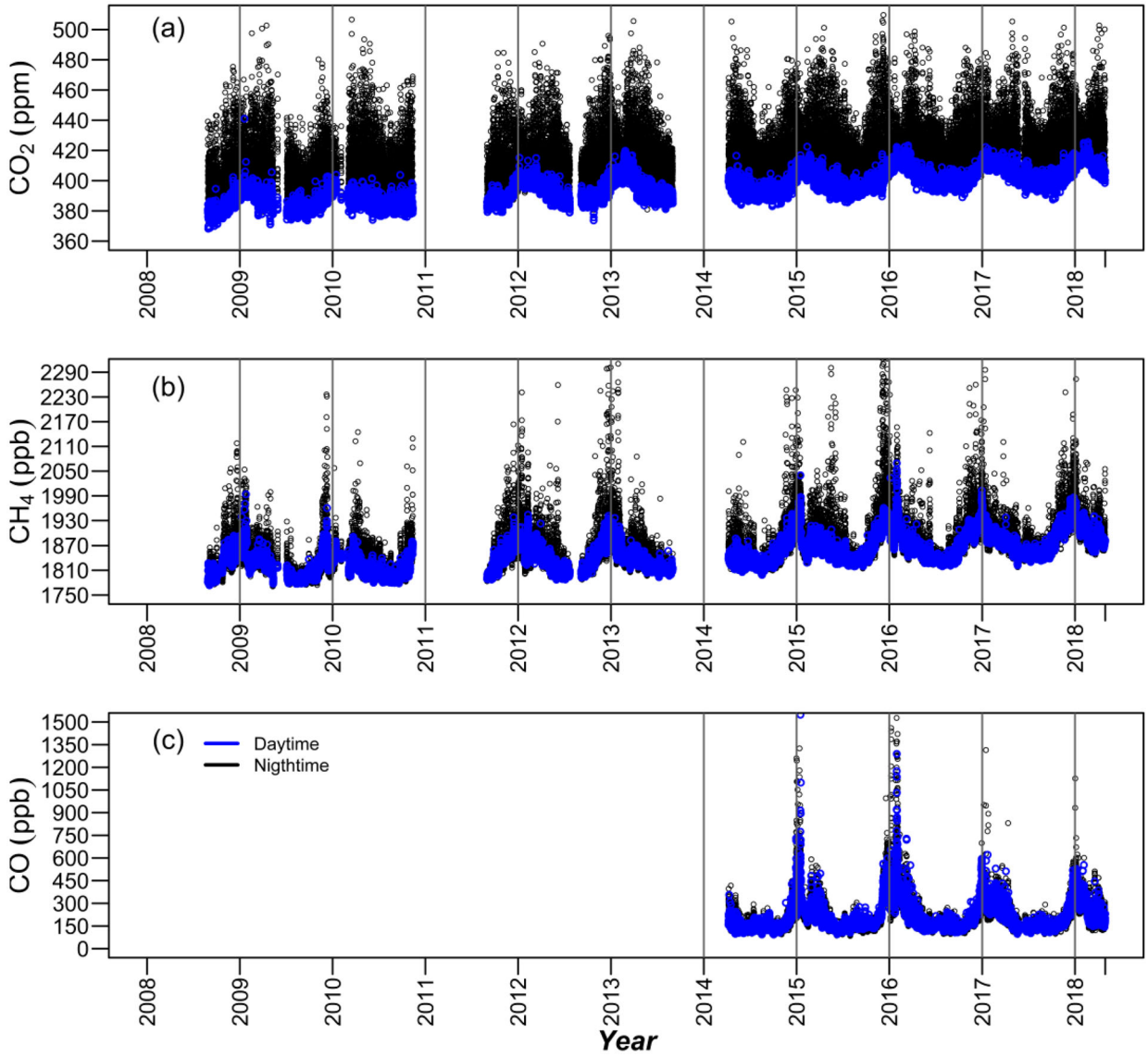


*Fig. 5.* Time series of atmospheric $CO_2$ (a), $CH_4$ (b) and CO (c) concentrations measured at the LTO station over the 2008-2018 period. The blue colour represents day-time data (from 11 h to 17 h) and the black colour represents night-time data (from 17 h to 11 h). The vertical lines differentiate years.

sources (e.g. biomass fires, wetlands) on the content of these compounds at LTO.

Figure 5c shows the time series of mean hourly CO concentrations from March 2014 to June 2018. Significant seasonal and interannual variabilities of CO concentrations are observed. The CO variations observed during the wet season from April to October are much smaller than the variations in the dry season from December-January-February (i.e. bushfire regime, agricultural slash-and-burn activities, etc.). The CO concentrations are in the range [83.69–5990.79] ppb, thus abnormally high values compared to those provided at clean air stations like Mt. Kenya-Kenya (MKT) or, Assekrem-Algeria (ASK) (WMO, 2017) mainly linked to biomass burning in the LTO region. About 1.5% of the hourly CO molar fractions values are lower than 150 ppb, 82% are between 150 and 350 ppb and 16% are higher than 350 ppb.

### 3.2. Diurnal cycle

The diurnal cycle of $CO_2$ in Fig. 6a shows a maximum concentration at 7 hr (local time) and a minimum between 14 hr and 17 hr during all the seasons. A gradual increase in

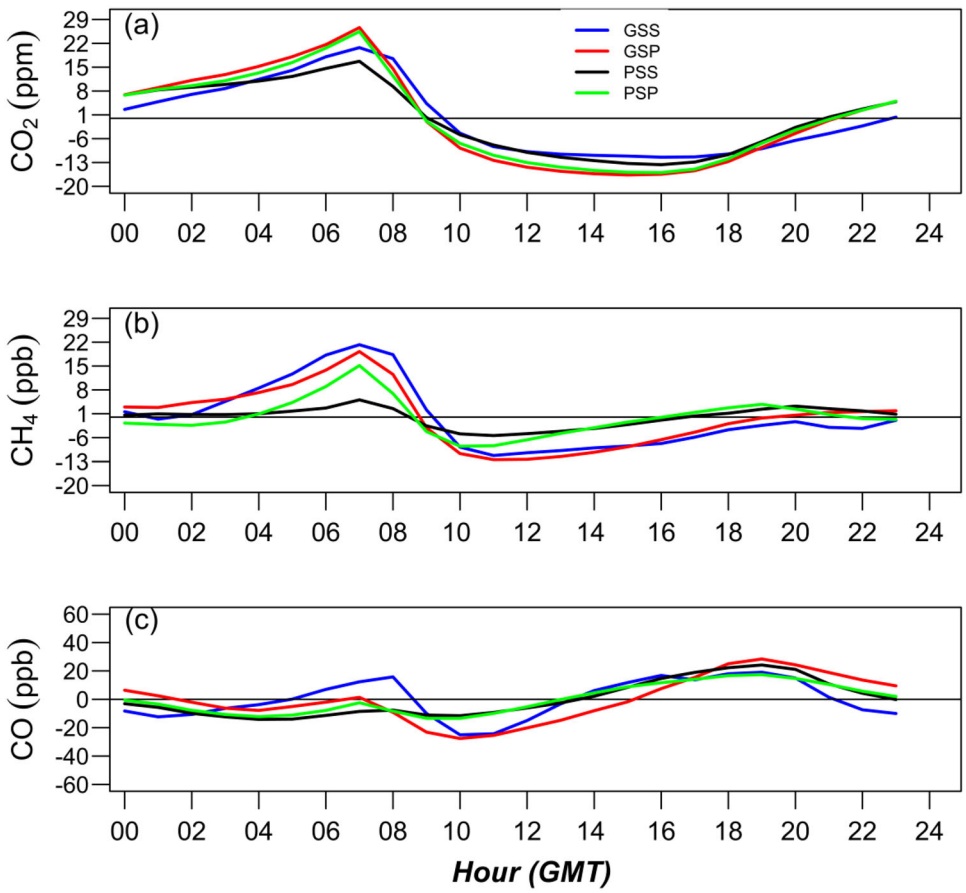


*Fig. 6.* Seasonal diurnal cycles of (a) $CO_2$, (b) $CH_4$ and (c) CO measured at Lamto (GMT) over the 2008-2018 period (for $CO_2$ and $CH_4$) and over the 2014-2018 period (for CO).

*Table 3.* Mean amplitudes of monthly diurnal variations of $CO_2$, $CH_4$ and CO at Lamto over the 2008–2018 period.

| Seasons | $CO_2$ (ppm) | $CH_4$ (ppb) | CO (ppb) |
|---|---|---|---|
| GSS | 36.69 | 29.82 | 32.51 |
| GSP | 43.27 | 31.75 | 56.03 |
| PSS | 30.37 | 10.48 | 38.31 |
| PSP | 41.40 | 23.70 | 30.79 |

concentrations starts towards 18 h and peaks in the morning. This signal can be explained by the combination of the variability of $CO_2$ fluxes exchanged between the vegetation, and the ABL (Putaud, 2019). Generally, ABL height increases after sunrise, reaches a maximum during noon, and decreases from sunset (Mahalakshmi et al., 2011; Mai et al., 2020). The accumulation of $CO_2$ at the surface stops abruptly after 7 hr, which result on the one hand from the radiative soil heating effects, which break up the inversion layer established during the night to mix vertically the trapped gases, and on the other hand reversal from $CO_2$ fluxes that become negative because of photosynthesis. $CO_2$ uptake by plants induces a slight decrease in $CO_2$ concentrations of ~4 ppm between 12 hr and 18 hrs when the atmospheric boundary layer is developed to altitudes between 1 and 2 km (Goudie and Middleton, 2001; Aryee et al., 2020; Mai et al., 2020; Pedruzo-Bagazgoitia et al., 2020). The highest amplitudes of the $CO_2$ diurnal cycle (peak to peak amplitude greater than 40 ppm) are observed during the rainy season GSP and PSP (Table 3).

The diurnal cycle of $CH_4$ in Fig. 6b shows a similar phase compared to $CO_2$, despite different surface fluxes, suggesting a dominant influence of the ABL. However, in contrast to $CO_2$, there is an increased concentration of $CH_4$ during the afternoon of about 8 ppb, after a minimum concentration reached around 12 hr, indicating daytime emissions of $CH_4$ in the footprint of the station, e.g. from the nearby dam. Although the phase of the diurnal cycle's changes very little from one season to another, their amplitudes show marked seasonal variations (Table 3). The largest diurnal amplitudes for $CH_4$ are observed during the main wet (GSP) and dry (GSS) seasons (Table 3).

The CO diurnal cycle is characterized by a double peak with two maxima, in the morning (7–8 hr) and the

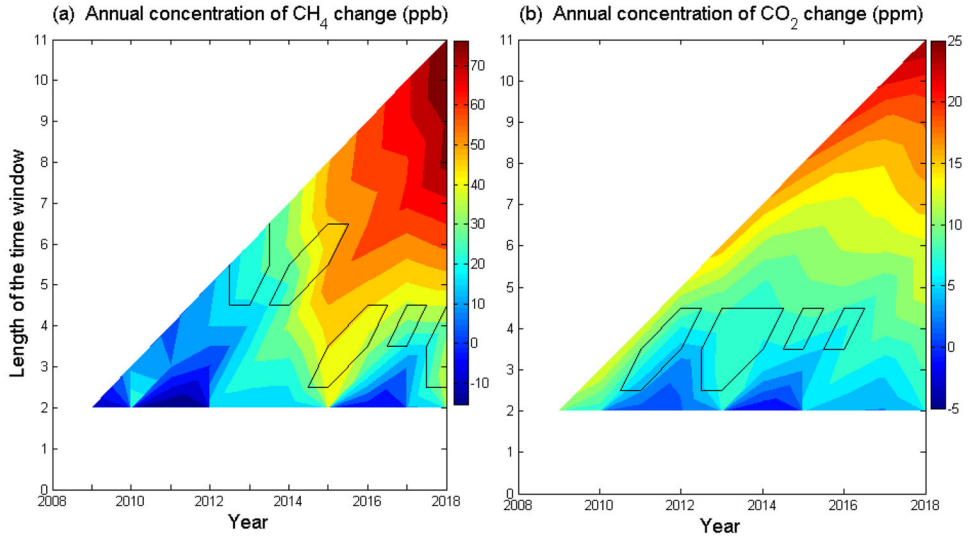


*Fig. 7.* Change of (a) $CH_4$ (ppb) and (b) $CO_2$ (ppm) concentrations recorded at the LTO station from May 2008 to August 2018 as a function of length of time window ($y$-axis) and ending of year of calculation. The inside of the black contours shows significant areas with a 95% confidence level from the student's $t$-test.

evening (18–20 hr), respectively. The causes of these peaks could result from the impact of the traffic occurring not far from the area, but the morning peak is probably related to accumulation near the surface just before ABL mixing decreases CO. The evening peak of CO is greater than the morning peak, possibly because of less convective evening boundary layer with evening denser traffic. The largest diurnal amplitude of CO is observed during the long rainy season (GSP), and the smallest during the short rainy season (PSP).

### 3.3. Growth rate of $CO_2$ and $CH_4$

Long-term trends and interannual variability of $CO_2$ and $CH_4$ have been calculated from the CCGvu software (Thoning et al., 1989). The mean growth rate of $CH_4$ over the 2008-2018 period is of 7 ppb year$^{-1}$, which is equal to the global mean growth rate obtained from marine boundary layer stations (Dlugokencky and Tans, 2020; https://www.esrl.noaa.gov/gmd/ccgg/trends_ch4/). The mean growth rate of $CO_2$ of 2.24 ppm year$^{-1}$ is close to the estimated global trend of 2.3 ppm year$^{-1}$ from marine sites (Dlugokencky and Tans, 2020; www.esrl.noaa.gov/gmd/ccgg/trends). In addition, further analysis of the $CH_4$ and $CO_2$ trends is illustrated in Fig. 7. This figure shows all trends for time segments of 2 to 11 years (total length of the time window), associated with a 95% confidence level by Student's $t$-test. Thus, it is obvious that time windows of several years or less may have an excess or a deficit of $CH_4$ or $CO_2$ concentrations. There is an increase and/or a decrease of concentrations during time segments shorter than 3 years for both $CH_4$ (Fig. 7a) and $CO_2$ (Fig. 7b), while for segments longer than 3 years, there is always an increase in concentrations (>8 ppb for CH4 and >5 ppm for $CO_2$). For example, the 8-year changes observed between 2009 and 2017 indicate an increase in $CH_4$ (∼+50 ppb) and $CO_2$ (∼+17 ppm) concentrations at Lamto region. Two variability modes (i.e. high and low frequency variability) are thus observed and characterise the trends of $CH_4$ and $CO_2$ concentrations. The low frequency variability (i.e. time segment ≥3 years) is associated only with an increase in $CH_4$ and $CO_2$ concentrations while the high frequency variability (i.e. time segment <3 years) is associated with relatively low positive and negative values. Furthermore, we note that the low frequency variability indicates significant positive trends for many time segments, while the high frequency variability shows two positive and significant trends for each compound, notably during 2015–2016 and 2017 for $CH_4$, and during 2010–2012 and 2012–2014 for $CO_2$.

Furthermore, Fig. 8 shows evolutions of the growth rates of $CO_2$ (Fig. 8a) and $CH_4$ (Fig. 8b) observed at the LTO, ASC, ASK, IZO and CVO stations during the 2008–2018 decade derived from daytime measurements. The annual growth rates of $CO_2$ from these different stations fluctuated from one year to the next, between 0.7 ppm yr$^{-1}$ and 4.20 ppm yr$^{-1}$. The long-term mean growth rate is, however, similar to the global average.

Highest $CO_2$ rates (>2.50 ppm yr$^{-1}$) were observed in 2010 at IZO and ASK, in 2015 and 2016 at IZO, ASK,

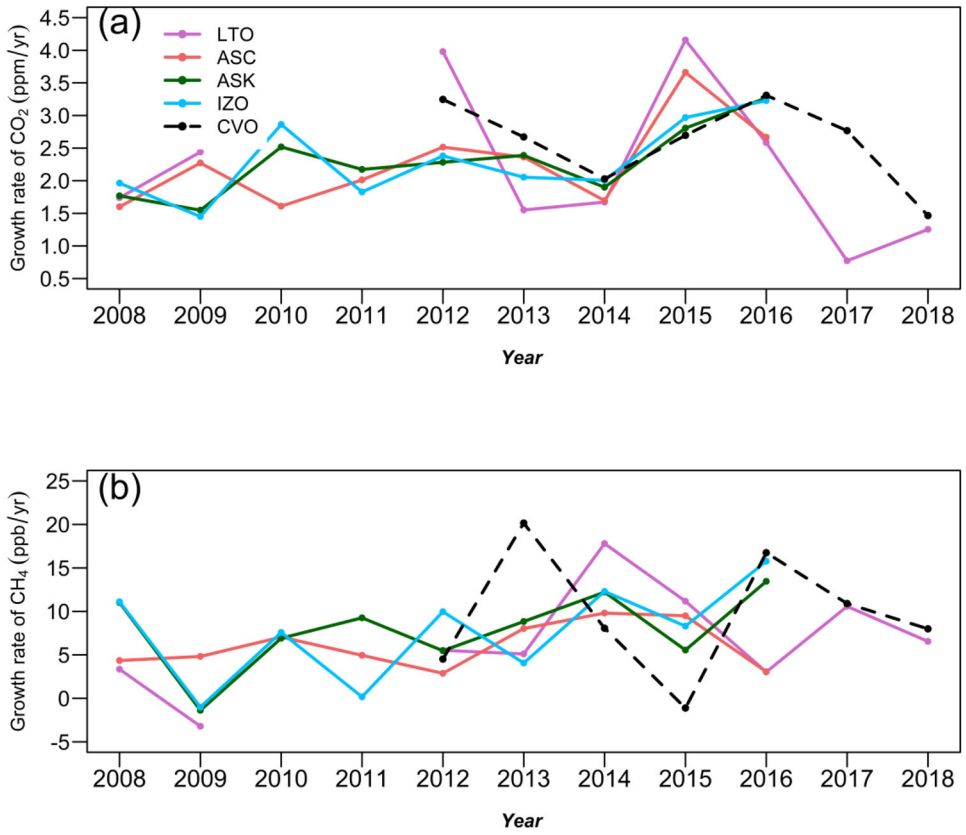


*Fig. 8.* Annual growth rate of $CO_2$ (a) and $CH_4$ (b) in the stations LTO, CVO, IZO, ASK et ASC. Due to lack of data, growth rates for some years are not presented.

ASC, CVO and LTO when the most severe El Nino Southern Oscillation (ENSO) event in this decade occurred. A similar result was found in studies of Patra et al. (2005) using 87 stations from 1959 to 2004. These studies have shown that the magnitudes of the observed $CO_2$ growth rate increase or decrease are mainly modulated by the ENSO variability. However, any analysis trying to characterize relationships between regional $CO_2$ growth rate and ENSO requires a longer time interval, which is not possible for the region of Western Africa. We observed a decrease in growth rates at LTO after the peak in 2015. This change may result in part from a decrease in precipitation, with a recovery of tropical vegetation after the 2015 El Nino. The $CO_2$ average annual growth rate at LTO was around 2.23 ppm. $yr^{-1}$, 1.5%, 2.7%, 3% and 16% lower than those observed at ASC, ASK, IZO and CVO, respectively. For $CH_4$, the growth rate shows a similar long-term mean across all stations with important interannual variability for LTO and CVO stations. This strong interannual variability observed at the CVO and LTO stations could be due to variable inter-annual air mass transport and flux exposure from the continent (Fomba et al., 2014; Tiemoko et al., 2020b). In addition, the average annual growth rate of $CH_4$ at LTO presents values ~6.65 ppb. $yr^{-1}$ that is 9% higher than that observed at ASC and 19%, 14% and 44% lower than those observed at ASK, IZO and CVO, respectively.

### 3.4. Seasonal cycles of $CO_2$, $CH_4$ and CO

*3.4.1. $CO_2$.* Figure 8 shows the smoothed curves derived from $CO_2$ observations over the last 10 years, and the mean seasonal cycles at the LTO, ASC, ASK, IZO and CVO stations.

The highest amplitude of the seasonal cycle is observed at LTO (13.6 ppm on average); ASK, IZO and CVO stations have a seasonal amplitude equivalent to half (~8 ppm peak-to-peak) of that of LTO, while AUC, which is located in the southern hemisphere and most often south of ITCZ, has an amplitude that is a quarter (~2.5 ppm peak-to-peak). The seasonal cycle at Lamto is characterized by a gradual decrease in $CO_2$ concentrations from January to July, followed by a broad minimum-till October and a rapid increase from November to January. On the other hand, the ASK, IZO and CVO

stations show seasonal cycles which are more typical of the background stations in the Northern mid-latitudes, with decreasing $CO_2$ concentrations from May to September followed by an increase in autumn (September to December) and a broad maximum in winter (December to March). This seasonality of the $CO_2$ cycle reflects the seasonality of the terrestrial vegetation fluxes and atmospheric transport. Also, the studies of Ago (2016) and Tiemoko et al.(2020a) on West African ecosystems indicated that photosynthesis is dominant during the rainy season and respiration exceeds it during the dry season. Compared to ASK, IZO and CVO, the maximum concentration at LTO occurs about 4 months earlier, in January. The LTO station is influenced by the biomass burning in West and Central Africa from December to February (Lacaux et al., 1995), and by the long-range transport of air masses from the north-east of the continent (Harmattan or boreal trade winds) coinciding with the fire season (Jonquières et al., 1998). Touré et al. (2012) showed that air masses from the north of the continent cross warm (i.e. Sahara) regions to reach the coastal areas of the Gulf of Guinea. These air masses contain dust and elevated levels of $CO_2$ from respiration and fire emissions. The decrease of $CO_2$ after January is probably related to the end of fire emissions with a dominant northerly wind regime (Kocha, 2011). The small secondary $CO_2$ peak observed in August could be due to the occurrence of the short dry season (Diawara et al., 2014) during which the respiration activity of plants is important.

*3.4.2. $CH_4$.* Figure 8e,f shows the $CH_4$ seasonal cycles at LTO, ASK, IZO and ASC stations. Mean annual molar fractions of $CH_4$ (Table 4) at LTO increased from 1822 ppb in 2008 to 1898 ppb in 2018. At LTO, ASK, IZO stations, the observed $CH_4$ concentrations show fairly similar seasonal cycles (Fig. 9e), with a larger amplitude in LTO. The $CH_4$ seasonal cycle at LTO shows a peak-to-peak amplitude of about 75 ppb, five times higher than in ASK (~13 ppb), 2.5 times higher than at IZO (~27 ppb) stations and practically similar in the CVO station. At the CVO station, the $CH_4$ seasonal cycle shows a peak in the month of April accompanied by a decrease until July followed by an increase starting in February. At LTO, there is a decrease of $CH_4$ concentrations from January to August-September, and an increase until December, similarly to the $CO_2$ seasonal cycle. This observed phase is in advance compared to the ASK and IZO stations, where the decrease in $CH_4$ concentrations occurs from March to June, and from March to July respectively. The decoupling of the LTO cycle compared to ASK, IZO and CVO in December and January is probably explained by $CH_4$ emissions from biomass burning, explaining the correlation with the $CO_2$ and CO cycles at Lamto. The seasonal variations in $CH_4$ concentrations are also related to changes in the OH concentration, which is the major $CH_4$ sink (Dlugokencky et al., 1994; Henne et al., 2008; McNorton et al., 2016). Satar et al. (2016) and Xia et al. (2020) showed, for example, that in the northern hemisphere, the $CH_4$ chemical elimination and atmospheric dilution peak in summer, which is the period when low $CH_4$ concentrations are measured. At the LTO station, this period extends from May to September and has significant cloud cover whose persistence induces low temperatures followed shortly afterwards by a drop in rainfall (Fig. 2) not favouring $CH_4$ emissions from biogenic sources.

*3.4.3. CO.* In the Lamto region, the most important sources of CO emissions are biofuels (i.e. firewood, charcoal, residues from agriculture), photodegradation of litter and wildfires. Seasonality and observed trends of CO at LTO, ASC, ASK, IZO and CVO are shown in Fig. 9c,d, respectively. In the case of the LTO station, there is a strong seasonal and interannual variability in CO. The highest concentrations are observed in January during the peak of the fire season (monthly average up to 450 ppb), while minimum concentrations are recorded between May and November (down to 130 ppb). At ASK, IZO, ASC and CVO, the mean monthly concentrations measured are systematically lower than 120 ppb and vary little from one month to another, compared to LTO. The mean annual molar fraction measured at LTO is $216 \pm 97$ ppb over the 2014–2018 period (Table 4 and Fig. 10d), and is above those observed at the other stations with differences of $140 \pm 89$ ppb, $116 \pm 86$ ppb, $118 \pm 82$ ppb and $117 \pm 85$ ppb ppb from ASC, ASK, IZO and CVO, respectively. The differences observed in CO concentrations between LTO and the other three stations are likely explained by sources of CO emissions (e.g. biofuels, biomass fires) in the Lamto region, particularly wildfires during the dry season from December to February. These sources of emission are both local and regional. Indeed, CO concentration levels at LTO are influenced by the transport of polluted air, especially during the great dry season when air masses from the north cross-areas where agricultural activities and fires are high. On the other hand, the ASC, ASK, IZO and CVO stations are far from sources of emission (biofuel, biomass combustion, etc.). Also, there are strong similarities between the CO and $CO_2$ seasonal cycles at Lamto that reflect a strong contribution of combustion sources in the $CO_2$ seasonal cycle at Lamto.

*Table 4.* Mean annual values and peak-to-peak amplitudes of $CO_2$, $CH_4$ and CO measured concentrations at LTO, ASC, ASK, IZO and CVO stations over the 2008–2018 period.

| | | LTO | ASC | ASK | IZO | CVO |
|---|---|---|---|---|---|---|
| | | | $CO_2$ (ppm) | | | |
| Annual mean | 2008 | 381 ± 4.84 | 385.54 ± 1.33 | 385.85 ± 2.60 | 385.75 ± 2.25 | – |
| | 2009 | 386.25 ± 4.68 | 385.55 ± 1.45 | 387.69 ± 2.75 | 387.09 ± 4.10 | – |
| | 2010 | 390.78 ± 3.88 | 387 ± 1.06 | 389.90 ± 2.73 | 389.41 ± 1.99 | – |
| | 2011 | 391.56 ± 6.56 | 389.19 ± 1.31 | 392.32 ± 2.72 | 391.74 ± 2.71 | – |
| | 2012 | 392.41 ± 5.32 | 391.50 ± 1.01 | 394.81 ± 3.16 | 393.99 ± 2.25 | 392.71 ± 0.33 |
| | 2013 | 396.88 ± 7.19 | 394.23 ± 1.21 | 397.41 ± 3.33 | 396.19 ± 2.38 | 399.45 ± 2.98 |
| | 2014 | 394.35 ± 3.20 | 395.98 ± 1.10 | 399.53 ± 3.27 | 398.04 ± 2.35 | 398.76 ± 2.88 |
| | 2015 | 398.92 ± 5.03 | 398.44 ± 1.12 | 402.03 ± 3.90 | 400.26 ± 1.99 | 400.21 ± 2.76 |
| | 2016 | 403.17 ± 5.21 | 402.21 ± 0.94 | 402.99 ± 2.44 | 403.95 ± 2.42 | 403.89 ± 3 |
| | 2017 | 404.37 ± 5.50 | – | – | – | 407.08 ± 2.58 |
| | 2018 | 410.90 ± 3.72 | – | – | – | 408.56 ± 2.96 |
| | Period | 396.47 ± 4.97 | 392.03 ± 1.17 | 394.32 ± 2.99 | 394.05 ± 2.50 | 401.10 ± 2.51 |
| | | | $CH_4$ (ppb) | | | |
| Annual mean | 2008 | 1822.29 ± 28.95 | 1752.32 ± 7.21 | 1815.58 ± 9.67 | 1824.27 ± 12.55 | – |
| | 2009 | 1820.07 ± 26.14 | 1756.06 ± 9.26 | 1824.09 ± 5.63 | 1829.73 ± 14.32 | – |
| | 2010 | 1825.12 ± 17.01 | 1762.17 ± 8.11 | 1821.56 ± 4.85 | 1834.91 ± 9.30 | – |
| | 2011 | 1838.45 ± 47.05 | 1768.35 ± 8.88 | 1831.60 ± 5.79 | 1836.39 ± 13.83 | – |
| | 2012 | 1839.05 ± 29.72 | 1772.00 ± 7.23 | 1840.16 ± 10.16 | 1844.27 ± 13.77 | 1861.98 ± 7.31 |
| | 2013 | 1835.55 ± 25.84 | 1776.82 ± 8.87 | 1848.98 ± 9.23 | 1850.71 ± 9.46 | 1854.46 ± 10.67 |
| | 2014 | 1843.76 ± 27.82 | 1786.77 ± 10.17 | 1859.89 ± 12.48 | 1857.33 ± 9.46 | 1878.95 ± 43.61 |
| | 2015 | 1866.74 ± 31.21 | 1796.05 ± 11.37 | 1867.46 ± 9.76 | 1866.26 ± 13.14 | 1875.497 ± 13.85 |
| | 2016 | 1871.72 ± 33.50 | 1802.62 ± 9.49 | 1873.66 ± 10.15 | 1881.43 ± 13.52 | 1910.89 ± 55.25 |
| | 2017 | 1880.07 ± 31.46 | – | – | – | 1889.66 ± 14.56 |
| | 2018 | 1898.43 ± 21.04 | – | – | – | 1903.13 ± 10.07 |
| | Period | 1853.07 ± 28.41 | 1774.79 ± 8.95 | 1841.77 ± 8.63 | 1847.26 ± 12.15 | 1882.04 ± 30 |
| | | | CO (ppb) | | | |
| Annual mean | 2008 | – | 74.19 ± 11.39 | 100.42 ± 13.65 | 101.75 ± 15.82 | – |
| | 2009 | – | 70.92 ± 10.02 | 98.27 ± 12.20 | 98.35 ± 16.37 | – |
| | 2010 | – | 81.77 ± 12.01 | 99.08 ± 9.36 | 105.13 ± 17.48 | – |
| | 2011 | – | 81.72 ± 6.95 | 99.69 ± 12.92 | 97.61 ± 16.93 | – |
| | 2012 | – | 77.57 ± 5.22 | 99.31 ± 10.40 | 98.48 ± 9.70 | 110.08 ± 9.96 |
| | 2013 | – | 78.53 ± 6.75 | 98.48 ± 10.91 | 95.04 ± 13.31 | 98.24 ± 11.64 |
| | 2014 | 160.94 ± 48.37 | 72.43 ± 7.97 | 98.57 ± 10.59 | 94.17 ± 11.26 | 97.10 ± 11.95 |
| | 2015 | 213.96 ± 91.48 | 71.81 ± 10.35 | 101.79 ± 11.36 | 95.82 ± 13.65 | 98.30 ± 11.29 |
| | 2016 | 226.53 ± 110.92 | 72.85 ± 6.96 | 97.02 ± 9.84 | 99.76 ± 16.87 | 99.56 ± 13.67 |
| | 2017 | 260.28 ± 71.91 | – | – | – | 97.78 ± 12.02 |
| | 2018 | 226.53 ± 110.92 | – | – | – | 94.82 ± 9.19 |
| | Period | 216.15 ± 96.94 | 75.76 ± 7.45 | 99.56 ± 10.75 | 98.46 ± 13.99 | 99.41 ± 11.40 |

The mean annual values and peak-to-peak amplitudes are calculated from the smoothed curve and the mean seasonal cycle of each gas.

### 3.5. Synoptic variations

In this section, we analyse the synoptic-scale variations of $CO_2$, $CH_4$ and CO by looking more specifically to the correlation's residual values (i.e. $\Delta CO_2$, $\Delta CH_4$ and $\Delta CO$) from the smoothed seasonal cycle (see Section 2.3.3). In this analysis we have been using only the mid-afternoon measurements (blue points on Fig. 5).

*3.5.1. $\Delta CO_2/\Delta CO$.* The monthly ($\Delta CO_2/\Delta CO$) slopes are calculated using regression lines orthogonal distance (i.e. Deming regression) over the 2014–2018 period. The numbers in red (Fig. 10a) are the correlation coefficients ($R$) between $CO_2$ and CO residues. These correlation coefficients are low, positive and significant ($R < 0.50$, $p < 0.001$) in all months except in July, which presents a

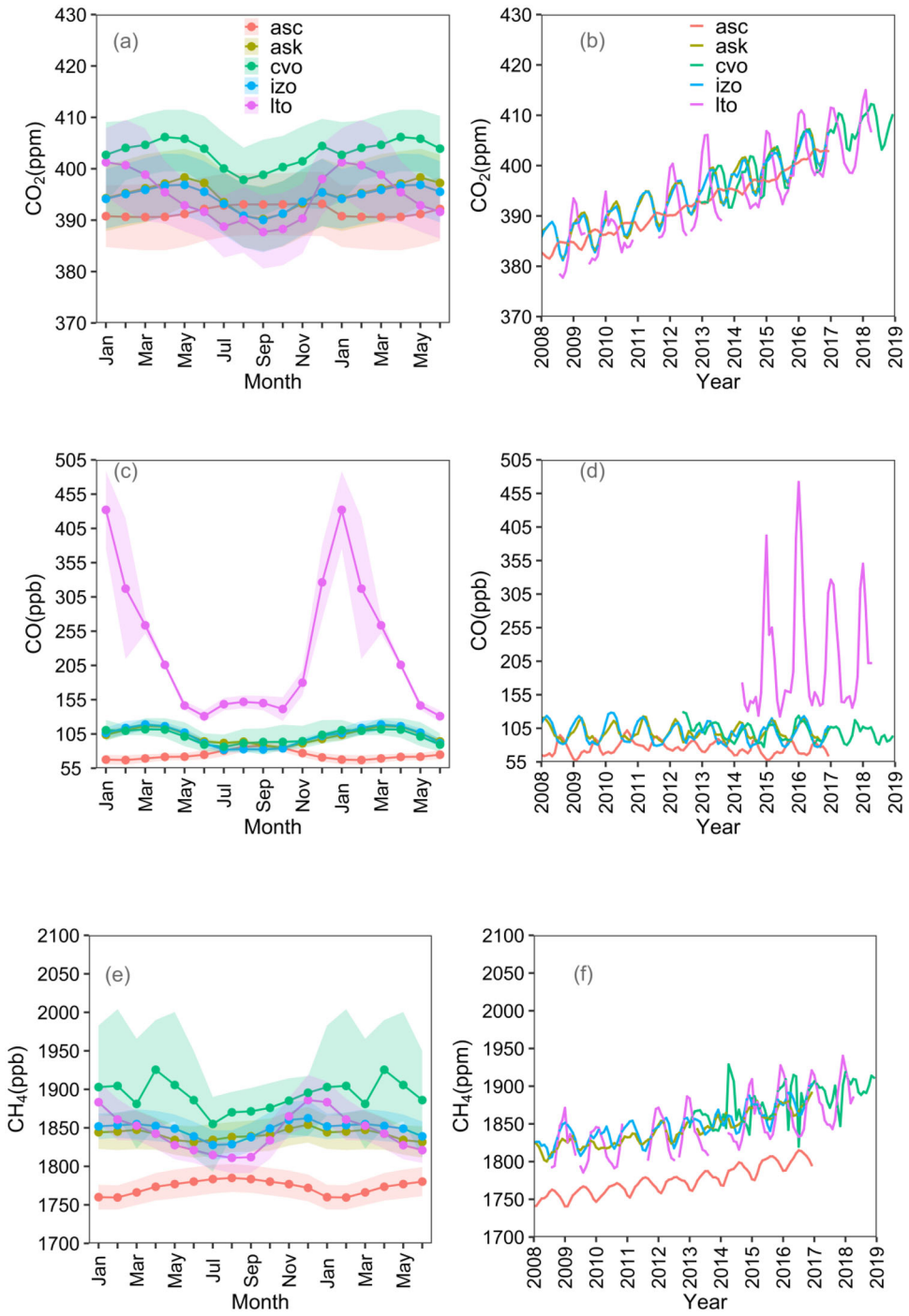


*Fig. 9.* Mean monthly variations and year-to-year trends of the (a and b) $CO_2$, (c and d) CO and (e and f) $CH_4$ molar fractions observed at the LTO station over the 2008–2018 period compared to those obtained at the ASC, ASK, IZO and CVO stations. It is noted that this analysis is based on daytime data only. Shaded areas of colour represent the estimated uncertainty in the average annual seasonal cycle. This estimate is based on the standard difference between the monthly mean values.

high and significant correlation value ($R = 0.56$, $p < 0.001$). ($R = 0.56$, $p < 0.001$). The low correlation coefficients show that changes in CO anomalies cannot explain those of $CO_2$. The atmospheric $CO_2$ variations are significantly controlled by plant uptake and respiration at very short time scales (Murayama et al., 2003).

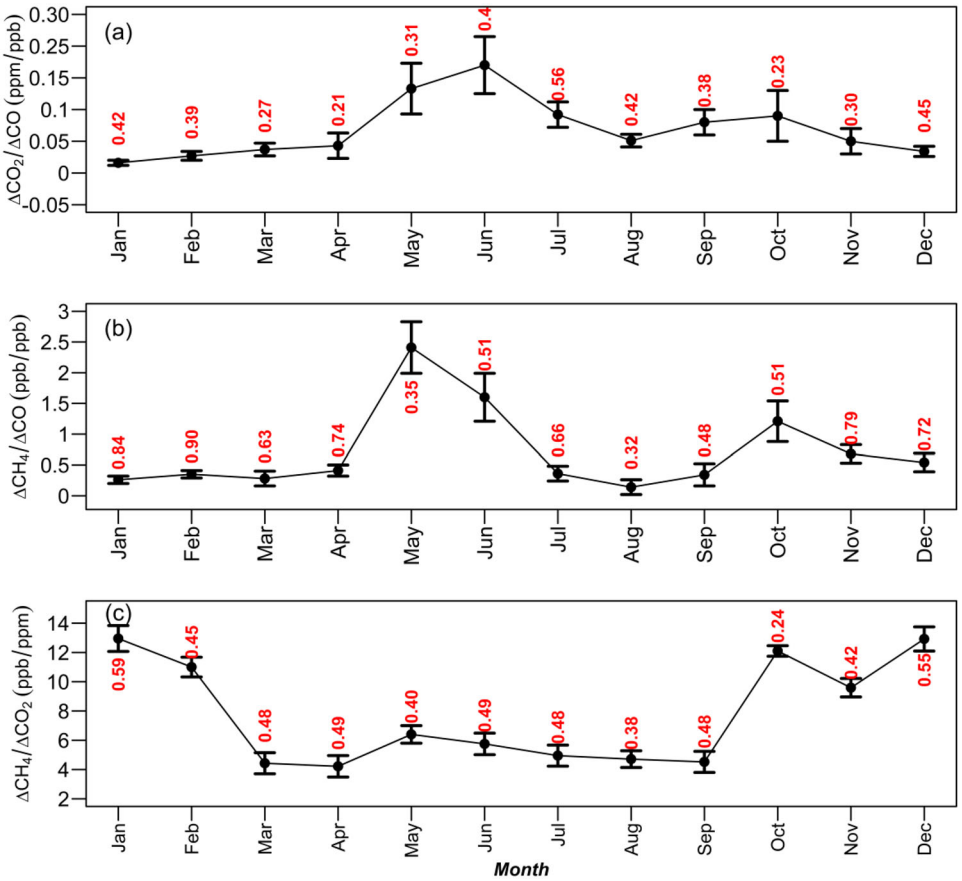


*Fig. 10.* Mean monthly variations (in black lines) of (a) $\Delta CO_2/\Delta CO$, (b) $\Delta CH_4/\Delta CO$ and (c) $\Delta CH_4/\Delta CO_2$ obtained from the dispersion pattern slopes between the $CO_2$, $CH_4$ and CO residues at the LTO station over the 2014-2018 period. The numbers in red are the correlation coefficients between each pair of species. Vertical black bars represent standard deviation.

As illustrated by the diel cycles, the magnitude of $CO_2$ variance driven by surface exchange with soils and vegetation exceeds the variance from combustion sources and has little impact on CO, hence relatively low correlations are observed. We notice that respiratory $CO_2$ from soils decreased with low temperatures and the unavailability of water in July, which could explain the higher correlation. The $\Delta CO_2/\Delta CO$ ratio is characterized by significant seasonal variations as shown in Fig. 10a, with high values outside the fire season between May (0.13 ppm $ppb^{-1}$) and July (09 ppm $ppb^{-1}$) on the one hand, and between September (0.08 ppm $ppb^{-1}$) and October (0.09 ppm $ppb^{-1}$) on the other hand. In August and the November-April season, $\Delta CO_2/\Delta CO$ ratios take lower values in the range of 0.02–0.05 ppm $ppb^{-1}$. This seasonal distribution of the $\Delta CO_2/\Delta CO$ variations follows the one of the rainfall patterns in the Lamto region characterized by alternating dry and wet seasons (Diawara et al., 2014). The low values of the concentration ratios recorded in the dry season also correspond to the influence of fires which provide high CO to $CO_2$ emission factors. Although CO is an important tracer of biomass combustion (Langenfelds et al., 2002), its short lifetime does not enable to fully explain (inconsistent coefficients of correlation) changes in recorded $CO_2$ fluxes during this season. The different components of $CO_2$ emissions from fires, but also from respiration after the fire period, causes uncertainties on the characterization of emission factors from $\Delta CO_2/\Delta CO$ concentration ratios. However, general estimates of fire emission rates are often used to characterize the nature of $CO_2$ emissions assuming that the observed enhancements of CO are mainly due to biomass fires (Suntharalingam, 2004; Henne et al., 2008; Wada et al., 2011; Denjean et al., 2020) The emission ratios (i.e., $\Delta CO_2/\Delta CO$) of combustion sources (Christian, 2003; Koppmann et al., 2005; Wada et al., 2011), for African savannas are estimated between 0.0031 and 0.032 ppm $ppb^{-1}$. During the FOS/DEFACE experiment in Lamto

(Côte d'Ivoire), Bonsang et al. (1995) reported molar ratios of $\Delta CO/\Delta CO_2$ in the range of 0.004 to 0.012 ppm $ppb^{-1}$. In the present study, the mean $\Delta CO_2/\Delta CO$ ratio estimated during the biomass burning period is 0.025 ppm $ppb^{-1}$ (0.034 ppm $ppb^{-1}$ in December, 0.016 ppm $ppb^{-1}$in January and 0.027 ppm $ppb^{-1}$in February), in agreement with Koppmann et al. (2005). The difference with the results of Bonsang et al. (1995) could be explained by the fact that these measurements and other such studies measured emission factors directly in fire plumes, whereas our data mix the signature of fires, respiration and regional background concentrations. In the LTO area, Diawara et al. (2014) showed that in particular years, the climate of Lamto can alternate between climate of arid region (i.e. dry savanna) and climate of sub-humid or humid region (i.e. humid savanna) with year to year variations of fire intensity, distribution and CO to $CO_2$ emission ratios. However, additional differences between biofuels types, fire intensity, firewood, charcoal and agricultural residues CO to $CO_2$ emission factors could also contribute to the variance of $\Delta CO_2/\Delta CO$ slopes at LTO.

*3.5.2. $\Delta CH_4/\Delta CO$.* Figure 9b shows the mean seasonal variations of the $\Delta CH_4/\Delta CO$ concentration ratios at LTO over the 2014–2018 period. The maximum ratio is observed in May (2.4 ppb $ppb^{-1}$), while the minimum values are in January (0.26 ppb $ppb^{-1}$), February (0.30 ppb $ppb^{-1}$) and August (0.14 ppb $ppb^{-1}$) in agreement with the range found in the literature on forest and savanna fire emission ratios ranging from 1 to 17%, i.e. 0.02 to 0.30 ppb $ppb^{-1}$ (Ward et al., 1982; Hurst et al., 1994; Koppmann et al., 2005). The seasonality in the ratios is likely dominated by the seasonality in CO emissions reaching its maximum in December-January-February (Fig. 9). The correlation coefficients between $\Delta CH_4$ and $\Delta CO$ are high and significant ($R > 0.5$, $p < 0.001$) in all months except in May ($R = 0.35$, $p < 0.001$), August ($R = 0.32$, $p < 0.001$) and September ($R = 0.48$, $p < 0.001$), unlike those obtained between $\Delta CO_2$ and $\Delta CO$. This observation shows that $CH_4$ and CO are closely related and moreover these positive coefficients suggest that the anthropogenic emissions and fires dominate the carbon cycle at the Lamto station. The periods corresponding to the high CO emissions also coincide with the periods of high values of the correlation coefficients ($R > 0.6$, $p < 0.001$) between $\Delta CH_4$ and $\Delta CO$. High values of correlation coefficients ($R > 0.5$, $p < 0.001$) between $\Delta CH_4$ and $\Delta CO$ indicate similar sources of emission (i.e. fire emissions) for these two gases (Fang et al., 2015).

Significant variations in $\Delta CH_4/\Delta CO$ concentration ratios are also observed during the wet seasons in April-July (GSP) and September-November (PSP). The ratios observed during those periods reflect significant $CH_4$ emissions compared to CO, while the smaller ratios observed in December-March (GSS) and August (PSS) indicate significant CO emissions compared to $CH_4$. The predominance of $CH_4$ or CO is established according to the rainfall regime at Lamto. The calculated concentration ratios vary between 0.26 ppb $ppb^{-1}$ and 2.41 ppb $ppb^{-1}$ and are for some months different to the provided regional (Bonsang et al., 1995; Pak, 2000; Koppmann et al., 2005; Lin et al., 2015) and global ratios (Xiao, 2004).This difference could be induced by the fact that the Lamto area is in the transition area between forest and savanna, seasonally influenced by large scale transport from the West African Monsoon (WAM) and Harmattan winds in the main dry season, but also by strong anthropogenic pressures (i.e. agricultural activities, burning, farming, etc.). As a result, seasonal cycles of CO and $CH_4$ potential sources of emissions may differ from a region to another considering the environment. To go further in this analysis, and to have a better estimate of regional emissions of these gases from the values of the concentration ratios, it would be interesting to have specific emission inventory that we could use in parallel with a source-receptor relationship method. In addition, $CH_4$ isotopic measurements could also be used to identify the influence of the dominant sources from biogenic vs. biomass burning origins (Bergamaschi et al., 1998; Mikaloff Fletcher et al., 2004; Barker et al., 2020).

*3.5.3. $\Delta CH_4/\Delta CO_2$.* Figure 9c shows the seasonal variations of the $\Delta CH_4/\Delta CO_2$ ratio and correlation coefficients between $\Delta CH_4$ and $\Delta CO_2$ over the 2014–2018 period. The slopes between $\Delta CH_4$ and $\Delta CO_2$ show significant seasonal variations ranging from 4.2 to 13 ppb $ppm^{-1}$, with an average of 7.8 ppb $ppm^{-1}$. This mean value is low compared to those calculated for anthropogenic emissions in North Africa (39.1 to 46.2 ppb $ppm^{-1}$), but relatively similar to that reported by Lacaux et al. (1995) (0.31% or 8.5 ppb $ppm^{-1}$) in biomass burning plumes in the tropical savannas of Côte d'Ivoire. The molar ratios of fire emissions found by Bonsang et al. (1995), during the FOS/DEFACE experiment at Lamto from December to February, range 0.32 to 0.46% (11 to 21.5 ppb $ppm^{-1}$) for fires with high combustion efficiency, is in accordance with the range (11 to 13 ppb $ppm^{-1}$) that we obtain during the fire season (i.e. from December to February) (Fig. 10c).We note that the average value obtained in Lamto (7.8 ppb $ppm^{-1}$) is relatively close to the concentrations found in suburban areas (7.1 ppb $ppm^{-1}$) in India by Sreenivas et al. (2016) and in the Los Angeles megacity (6.4 ppb $ppm^{-1}$) by Wong et al. (2014). These authors underlined that the $\Delta CH_4/\Delta CO_2$ low values indicate

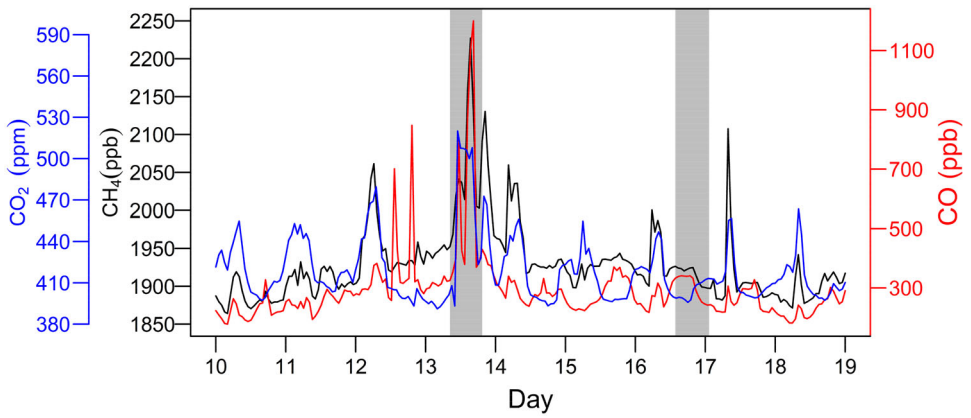


*Fig. 11.* Hourly variations of CO (red), $CO_2$ (blue) and $CH_4$ (black) concentrations from 10 to 19 December 2014 observed at the LTO station. Vertical gray shading corresponds to periods of high (December 13, 2014) and low (December 16–17, 2014) $CO_2$, $CH_4$ and CO concentration values that appear simultaneously and for which back-trajectories have been traced.

dominance of $CO_2$ anthropogenic emissions in the studied area. On the other hand, October (12.1 ppb $ppm^{-1}$), November (9.59 ppb $ppm^{-1}$), December (12.92 ppb $ppm^{-1}$), January (12.95 ppb $ppm^{-1}$) and February (11.0 ppb $ppm^{-1}$) record higher $\Delta CH_4/\Delta CO_2$ concentration ratios than the average rate, indicating the dominance of $CH_4$ during these months. This dominance shows that local to regional emissions influencing the LTO station are probably controlled by fire emission in these months. The molar emission rates overall observed for different biomass burning events in various ecosystems range from lowest values of about 0.1% to highest values of about 2% (i.e. 2.75 to 55 ppb $ppm^{-1}$)depending on the biofuel and the phase of the fire (Greenberg et al., 1984; Crutzen et al., 1985; Cofer et al., 1990; Bonsang et al., 1991; Kaufman et al., 1992; Hurst et al., 1994; Lacaux et al., 1995; Yokelson et al., 1997; Pak, 2000; Koppmann et al., 2005). The molar fractions calculated in our study are within the large range provided by these authors. Moreover, the calculated correlations show positive and significant values ($p < 0.001$) between 0.24 and 0.59. The correlations lower than 0.5 are obtained from February to November and those higher than 0.5 in December and January (12.9 ppb $ppm^{-1}$). Strong correlations (>0.5) indicate that the factors which control the emissions and variability of $CH_4$ and $CO_2$ in December and in January, could be similar, especially as their molar fractions vary in the same way. On the other hand, the very tight correlations suggest that biospheric $CO_2$ fluxes play only a minor role and that the ratios are dominated by collocated anthropogenic emissions and fires of $CH_4$ and $CO_2$. Fang et al. (2015) suggested similar patterns of $CO_2$ and $CH_4$ sources for correlation coefficients greater than 0.5. Hence, the observed correlation between $\Delta CH_4$ et $\Delta CO_2$ in this study during December-January is not only due to spatially and temporally correlated sources but is caused to a large extent by meteorological variability associated with more or less accumulation of trace gases in the boundary layer irrespective of their sources. In conclusion the processes controlling both $CH_4$ and $CO_2$ emissions during February-November are heterogeneous.

### 3.6. Case study from December 10 to 19, 2014

Figure 11 shows the $CO_2$, $CH_4$ and CO concentrations recorded at Lamto from December 10th to 21st 2014. The observed signals of these three species show typical variations at the scale of a few hours and a few days. For $CO_2$ we observe systematically night-time increase with a large amplitude (40 to 120 ppm). $CO_2$ peaks are generally associated with CO peaks, indicating a large contribution of emissions by combustion processes. $CH_4$ has less pronounced diurnal cycles, and sometimes in phase opposition with $CO_2$ and CO (e.g. Dec. 16–17). Superimposed on the diurnal cycles, we observe a significant increase around 13 December, framed by two periods of lesser variability and lower concentrations. The co-occurrence of this peak of $CO_2$, $CH_4$ and CO at Lamto suggests influences of polluted air masses with common sources and origins. The determination of the contribution of regional and/or distant sources on the levels of $CO_2$, $CH_4$ and CO concentrations observed passes necessarily by identification of the origin of the air masses arriving at the station. For this purpose, we calculated three-day back trajectories of air masses above Lamto (Figs. 12 and 13) coinciding with observed peaks (December 13, 2014) and the period of low concentrations (December 16-17, 2014) using the FLEXPART and HYSPLIT models

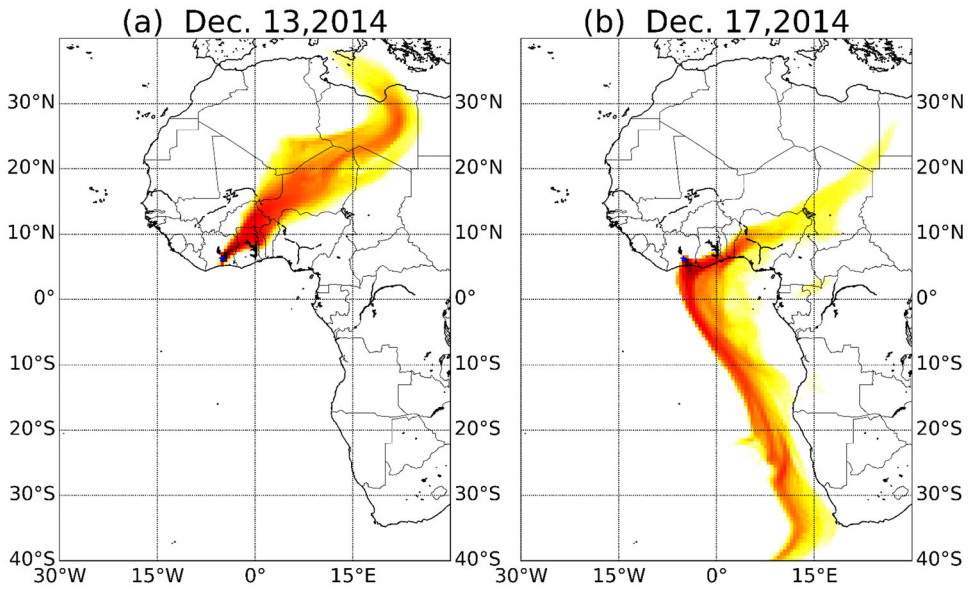


Fig. 12. Average footprints for air masses arriving at the station from December 16th to 17 h and from 13th to 14th. The Lagrangian Particle Dispersion Model (LPDM) FLEXPART Version 9.0 in backward mode, forced by ECMWF wind fields with 0.5° × 0.5° spatial and 3 h temporal resolution is used to simulate the footprints (Stohl et al., 1998 ; Berchet et al., 2015). Inverse simulation consists of 1000 particles released at 1-hourly times steps over a day from the Lamto sampling inlet position (lon = –5.0278, lat = 6.2244, alt = 50m) and followed ten days backward in time (following Paris et al., 2010).

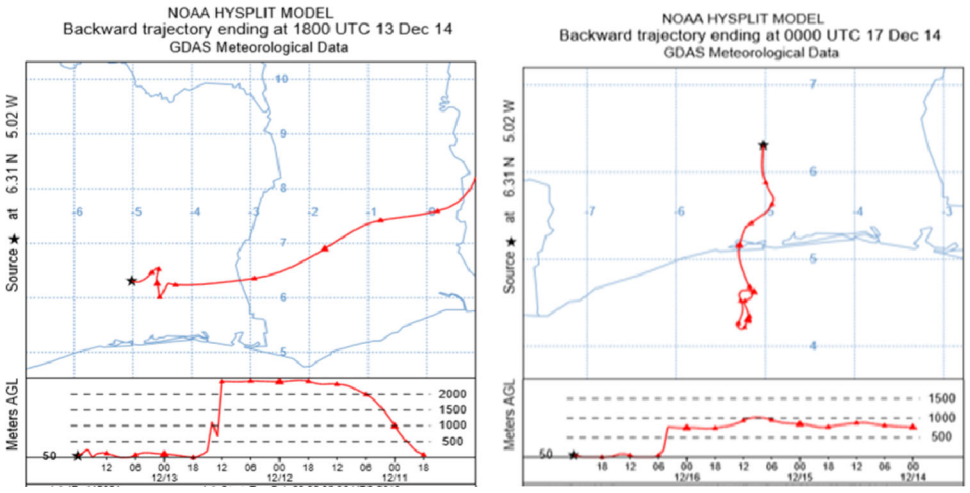


*Fig. 13.* 72-Hour retrotrajectoires of the air masses observed at the LTO station on 13 and 17 December 2014 with an altitude of 50 m based on the GDAS weather data. The LTO station is represented by a star. The upper part of the figure shows the ground trace of the air masses path and the lower part represents the altitude of the air masses during transport. The positions and altitude of the air masses are calculated every 6 hours.

(Draxler and Rolph, 2003). The back trajectories highlight two distinct origins: air masses coming from the East during the peak, indicating advection of polluted air coming from the continent, and coming from the South bringing cleaner air to the station on 17 December. It should be noted that even when the air mass is originating from the South, with the Atlantic Ocean located 165 km away, we still observe a significant $CO_2$ diurnal cycle generated by the biospheric activity and the correlation with the diurnal cycle of the boundary layer development. The eastern air masses from the continent may be influenced by emissions from cities in Ghana, but

also by biomass fires occurring during the dry season (van der Werf et al., 2010).

## 4. Conclusion and perspectives

The measured atmospheric $CO_2$, $CH_4$ and CO concentrations at LTO station were analyzed at different scales, from hours to the decade. The times series from August 2008 to June 2018 (for $CH_4$ and $CO_2$) and from 2014 to June 2018 (for CO) show a wide range of hourly mean concentrations ranging from 368 and 510 ppm for $CO_2$, from 1771 to 2350 ppb for $CH_4$ and from 84 to 5990 ppb for CO. Strong contrasts are generally observed between day time and night time values for all gases. We observe a sharp decrease in the concentrations around 7 hr in the morning, probably due to the effects of the soil radiative heating, which break the inversion layer formed during the night and releases the entrapped gases. The lowest variations in concentrations are observed during the wet season from April to October, whereas the highest variations appear during the bushfire regime (December-January-February).

Seasonal cycles compared to those of NOAA's stations (ASC, ASK, IZO) show stronger seasonal and interannual variability associated with the biomass fire regime from December to February, but also with long-distance air mass transport from the southern Atlantic (monsoon) and from the north-east of the continent (Harmattan). Besides, the $\Delta CO_2/\Delta CO$ concentration ratio variations are significant and show a seasonal coherence with the rainfall regime of the Lamto region but these values differ from those provided by over studies for African savannas. On the other hand, the $\Delta CH_4/\Delta CO$ ratios indicate significant $CH_4$ emissions with respect to CO during April-July and September-November, and significant CO emissions compared with $CH_4$ during December-March and August. The predominance of $CH_4$ or CO is thus established according to the rainfall regime at Lamto. The correlations between $CH_4$ and CO are positive and significant, indicating that the variations of these two gases are closely related. Also, the $\Delta CH_4/\Delta CO_2$ ratios have low values compared to those calculated in anthropogenic emissions in North Africa, Central Asia, and the Middle East region. The associated correlation coefficients indicate values greater than 0.5 in December and January with concentration ratios of 12.9 ppb $ppm^{-1}$. This means that during these two months the factors controlling the $CH_4$ and $CO_2$ emissions are similar.

This paper demonstrates the possibility of carrying out precise and long-term GHG measurements in Lamto, in a region of the world that previously had no continuous observation site. There is therefore no doubt that this station will provide valuable information on understanding GHG fluxes in West Africa using atmospheric inversions. Because ground level GHG data from this site may not capture the full transport of GHG and pollutants produced by fires, being uplifted in the troposphere e.g. by pyro-convection. For this reason, an analyzer (EM27/Sun) of total GHG columns will be installed at Lamto in 2021, which will allow a more complete view of the dispersion of biomass burning plumes during fire periods, and validation of satellite observations.

## Acknowledgements

We acknowledge the Laboratory of Climate Sciences and Environment (LSCE, CEA/CNRS/UVSQ), which provided the greenhouse gases analyzers, as part of the SNO-RAMCES/ICOS monitoring network. Thanks to NOAA/ESRL for sharing the observations from their global flask sampling network, and to University of Exeter for sharing the CVO observations. We also thank the anonymous reviewers for their helpful comments on this article.

## Disclosure statement

The authors declare that there are no conflicts of interest regarding the publication of this article.

## Funding

The authors thank the Programme Stratégique d'Appui à la Recherche Scientifique en Côte d'Ivoire (PASRES), the Centre d'Excellence Africain pour le Changement Climatique, la Biodiversité et l'Agriculture Durable (CEA-CCBAD) and the Geophysical Station of Lamto for their financial support. P.C. acknowledges support from the CLAND convergence institute of ANR.

## References

Abbadie, L., Gignoux, J., and Lepage, M. 2006. *Lamto: Structure, Functioning, and Dynamics of a Savanna Ecosystem. Springer Science & Business Media*, New York.

Ago, E. E. 2016. *Dynamique Des Flux De Carbone Entre L'atmosphère Et Des Ecosystèmes Ouest-Africains : cas Des Forêts Et Savanes Sous Climat Soudanien au Bénin*. Université de Liège Gembloux *Agro-Bio-Tech* (ULg), Liège.

Ago, E. E., Agbossou, E. K., Ozer, P. and Aubinet, M. 2016. Mesure des flux de $CO_2$ et séquestration de carbone dans les écosystèmes terrestres ouest-africains (synthèse bibliographique). *Biotechnol. Agron. Soc. Environ.* **20**, 15.

Andela, N. and van der Werf, G. R. 2014. Recent trends in African fires driven by cropland expansion and El Niño to La

Niña transition. *Nat. Clim. Change* **4**, 791–795. doi:10.1038/nclimate2313

Aryee, J. N. A., Amekudzi, L. K., Preko, K., Atiah, W. A. and Danuor, S. K. 2020. Estimation of planetary boundary layer height from radiosonde profiles over West Africa during the AMMA field campaign: Intercomparison of different methods. *Sci. Afr.* **7**, e00228.

Bakwin, P. S., Tans, P. P., Hurst, D. F. and Zhao, C. 1998. Measurements of carbon dioxide on very tall towers: Results of the NOAA/CMDL program. *Tellus B: Chemical and Physical Meteorology* **50**, 401–415. v50i5.16216. doi:10.3402/tellusb.v50i5.16216

Barker, P. A., Allen, G., Bannan, T., Mehra, A., Bower, K. N. and co-authors. 2020. Airborne measurements of fire emission factors for African biomass burning sampled during the MOYA Campaign. *Atmos. Chem. Phys.* **20**, 15443–15459. doi:10.5194/acp-20-15443-2020

Berchet, A., Pison, I., Chevallier, F., Paris, J.-D., Bousquet, P. and co-authors. 2015. Natural and anthropogenic methane fluxes in Eurasia: a mesoscale quantification by generalized atmospheric inversion. *Biogeosciences* **12**, 5393–5414. doi:10.5194/bg-12-5393-2015

Bergamaschi, P., Lubina, C., Königstedt, R., Fischer, H., Veltkamp, A. C. and co-authors. 1998. Stable isotopic signatures ($\delta^{13}C$, $^{\delta}D$) of methane from European landfill sites. *J. Geophys. Res.* **103**, 8251–8265. doi:10.1029/98JD00105

Bombelli, A., Henry, M., Castaldi, S., Adu-Bredu, S., Arneth, A. and co-authors. 2009. An outlook on the Sub-Saharan Africa carbon balance. *Biogeosciences* **6**, 2193–2205. doi:10.5194/bg-6-2193-2009

Bonsang, B., Boissard, C., Le Cloarec, M. F., Rudolph, J. and Lacaux, J. P. 1995. Methane, carbon monoxide and light non-methane hydrocarbon emissions from African savanna burnings during the FOS/DECAFE experiment. *J. Atmos. Chem.* **22**, 149–162. doi:10.1007/BF00708186

Bonsang, B., Lambert, G., and Boissard, C. C. 1991. Light hydrocarbon emissions from African savanna burnings. In: *Biomass Burning and Global Change* (ed. J. S. Levine). MIT Press, Cambridge, MA.

CEDEAO-CSAO/OCDE (Atlas de l'intégration Régionale en Afrique de l'ouest). 2008. *Le climat et les changements climatiques, série environnement, 2008.* https://www.oecd.org/fr/csao/publications/40121057.pdf

Chen, H., Winderlich, J., Gerbig, C., Hoefer, A., Rella, C. W. and co-authors. 2010. High-accuracy continuous airborne measurements of greenhouse gases ($CO_2$ and $CH_4$) using the cavity ring-down spectroscopy (CRDS) technique. *Atmos. Meas. Tech.* **3**, 375–386. doi:10.5194/amt-3-375-2010

Chevallier, F., Palmer, P. I., Feng, L., Boesch, H., O'Dell, C. W. and co-authors. 2014. Toward robust and consistent regional $CO_2$ flux estimates from in situ and space borne measurements of atmospheric $CO_2$. *Geophys. Res. Lett.* **41**, 1065–1070. doi:10.1002/2013GL058772

Christian, T. J. 2003. Comprehensive laboratory measurements of biomass-burning emissions: 1. Emissions from Indonesian, African, and other fuels. *J. Geophys. Res* **108**, 4719. doi:10.1029/2003JD003704

Ciais, P., Rayner, P., Chevallier, F., Bousquet, P., Logan, M. and co-authors. 2010. *Atmospheric Inversions for Estimating CO2 Fluxes: methods and Perspectives* (M. Jonas, Z. Nahorski, S. Nilsson, and T. Whiter, eds.). *Springer*, Netherlands, Dordrecht.

Cofer, W. R., Levine, J. S., Winstead, E. L. and Stocks, B. J. 1990. Gaseous emissions from Canadian boreal forest fires. *Atmos. Environ. Part A.* **24**, 1653–1659. doi:10.1016/0960-1686(90)90499-D

Conil, S., Helle, J., Langrene, L., Laurent, O., Delmotte, M. and co-authors. 2019. Continuous atmospheric $CO_2$, $CH_4$ and CO measurements at the Observatoire Pérenne de l'Environnement (OPE) station in France from 2011 to 2018. *Atmos. Meas. Tech.* **12**, 6361–6383. doi:10.5194/amt-12-6361-2019

Crosson, E. R. 2008. A cavity ring-down analyzer for measuring atmospheric levels of methane, carbon dioxide, and water vapor. *Appl. Phys. B.* **92**, 403–408. doi:10.1007/s00340-008-3135-y

Crutzen, P. J., Delany, A. C., Greenberg, J., Haagenson, P., Heidt, L. and co-authors. 1985. Tropospheric chemical composition measurements in Brazil during the dry season. *J. Atmos. Chem.* **2**, 233–256. doi:10.1007/BF00051075

Denjean, C., Bourrianne, T., Burnet, F., Mallet, M., Maury, N. and co-authors. 2020. Overview of aerosol optical properties over southern West Africa from DACCIWA aircraft measurements. *Atmos. Chem. Phys.* **20**, 4735–4756. doi:10.5194/acp-20-4735-2020

Diawara, A., Yoroba, F., Kouadio, K. Y., Kouassi, K. B., Assamoi, E. M. and co-authors. 2014. Climate variability in the sudano-guinean transition area and its impact on vegetation: The case of the Lamto region in Côte D'Ivoire. *Adv. Meteorol.* **2014**, 1–11. doi:10.1155/2014/831414

Dlugokencky, E. D. and Tans, P. 2020. *Recent Global $CO_2$.* www.esrl.noaa.gov/gmd/ccgg/trends/.

Dlugokencky, E. J., Steele, L. P., Lang, P. M. and Masarie, K. A. 1994. The growth rate and distribution of atmospheric methane. *J. Geophys. Res.* **99**, 17021. doi:10.1029/94JD01245

Draxler, R. R. and Rolph, G. D. 2003. *HySPLIT (Hybrid Single Particle Lagrangian Integrated Trajectory) Model Access via NOAA ARLREADY Website* (http://www.arl.noaa.gov/ready/hysplit4.html). NOAA Air Resources Laboratory, Silver Spring, MD.

Duren, R. M. and Miller, C. E. 2012. Measuring the carbon emissions of megacities. *Nature Clim. Change* **2**, 560–562. doi:10.1038/nclimate1629

Fang, S., Tans, P. P., Yao, B., Luan, T., Wu, Y. and co-authors. 2017. Study of atmospheric $CO_2$ and CH4 at Longfengshan WMO/GAW regional station: The variations, trends, influence of local sources/sinks, and transport. *Sci. China Earth Sci.* **60**, 1886–1895. doi:10.1007/s11430-016-9066-3

Fang, S. X., Tans, P. P., Steinbacher, M., Zhou, L. X. and Luan, T. 2015. Comparison of the regional CO2 mole fraction filtering approaches at a WMO/GAW regional station in China. *Atmos. Meas. Tech.* **8**, 5301–5313. doi:10.5194/amt-8-5301-2015

FAO. 2011. Situation des forêts du monde. *Organisation Des Nations Unies Pour L'alimentation Et L'agriculture.* Année Internationale Des Forêts : Rome, Italie. http://www.fao.org/3/i2000f/i2000f00.pdf

Fernández-Duque, B., Pérez, I. A., Sánchez, M. L., García, M. Á. and Pardo, N. 2017. Temporal patterns of $CO_2$ and $CH_4$ in a rural area in northern Spain described by a harmonic equation over 2010–2016. *Sci. Total Environ.* **593–594**, 1–9. doi:10.1016/j.scitotenv.2017.03.132

Fomba, K. W., Müller, K., van Pinxteren, D., Poulain, L., van Pinxteren, M. and co-authors. 2014. Long-term chemical characterization of tropical and marine aerosols at the Cape Verde Atmospheric Observatory (CVAO) from 2007 to 2011. *Atmos. Chem. Phys.* **14**, 8883–8904. doi:10.5194/acp-14-8883-2014

GIEC. 2014. *Changement Climatique 2014: rapport De Synthèse. Contribution Des Groupes De Travail I, II Et III au Cinquième Rapport D'évaluation du Groupe D'experts Intergouvernemental Sur L'évolution du Climat [Sous la Direction De L'équipe De Rédaction Principale* (R.K. Pachauri, L.A. Meyer, eds.). GIEC, Genève, Suisse, pp. 161.

Goudie, A. S. and Middleton, N. J. 2001. Saharan dust storms: nature and consequences. *Earth. Sci. Rev.* **56**, 179–204. doi:10.1016/S0012-8252(01)00067-8

Grant, A., Witham, C. S., Simmonds, P. G., Manning, A. J. and O'Doherty, S. 2010. A 15-year record of high-frequency, in situ measurements of hydrogen at Mace Head, Ireland. *Atmos. Chem. Phys.* **10**, 1203–1214. doi:10.5194/acp-10-1203-2010

Greenberg, J. P., Zimmerman, P. R., Heidt, L. and Pollock, W. 1984. Hydrocarbon and carbon monoxide emissions from biomass burning in Brazil. *J. Geophys. Res.* **89**, 1350. doi:10.1029/JD089iD01p01350

Guérette, E.-A., Paton-Walsh, C., Desservettaz, M., Smith, T. E. L., Volkova, L. and co-authors. 2018. Emissions of trace gases from Australian temperate forest fires: emission factors and dependence on modified combustion efficiency. *Atmos. Chem. Phys.* **18**, 3717–3735. doi:10.5194/acp-18-3717-2018

Harris, J. M., Dlugokencky, E. J., Oltmans, S. J., Tans, P. P., Conway, T. J. and co-authors. 2000. An interpretation of trace gas correlations during Barrow, Alaska, winter dark periods, 1986-1997. *J. Geophys. Res.* **105**, 17267–17278. doi:10.1029/2000JD900167

Henne, S., Klausen, J., Junkermann, W., Kariuki, J. M., Aseyo, J. O. and co-authors. 2008. Representativeness and climatology of carbon monoxide and ozone at the global GAW station Mt. Kenya in equatorial Africa. *Atmos. Chem. Phys.* **8**, 3119–3139. doi:10.5194/acp-8-3119-2008

Hurst, D. F., Griffith, D. W. T., Carras, J. N., Williams, D. J. and Fraser, P. J. 1994. Measurements of trace gases emitted by Australian savanna fires during the 1990 dry season. *J. Atmos. Chem.* **18**, 33–56. doi:10.1007/BF00694373

Jonquières, I., Marenco, A., Maalej, A. and Rohrer, F. 1998. Study of ozone formation and transatlantic transport from biomass burning emissions over West Africa during the airborne Tropospheric Ozone Campaigns TROPOZ I and TROPOZ II. *J. Geophys. Res.* **103**, 19059–19073. doi:10.1029/98JD00819

Karimou, B. M., Ambouta, K., Sarr, B. and Tychon, B. 2015. Analyse des Phénomènes Climatiques Extrêmes Dans le sud-est du Niger. XXVIIIe Colloque de l'Association Internationale de Climatologie, Liège. pp. 537–542.

Kaufman, Y. J., Setzer, A., Ward, D., Tanre, D., Holben, B. N. and co-authors. 1992. Biomass burning airborne and spaceborne experiment in the Amazonas (BASE-A). *J. Geophys. Res.* **97**, 14581. doi:10.1029/92JD00275

Kocha, C. 2011. *Interactions Entre Poussières Désertiques Et Convection Profonde En Afrique De L'Ouest : Observations Et Modélisation à Echelle Convective Météorologie*. Université Paul Sabatier - Toulouse III, France.

Koppmann, R., von Czapiewski, K. and Reid, J. S. 2005. A review of biomass burning emissions, part I: gaseous emissions of carbon monoxide, methane, volatile organic compounds, and nitrogen containing compounds. *Atmos. Chem. Phys. Discuss.* **5**, 10455–10516. doi:10.5194/acpd-5-10455-2005

Kouassi, K., Wognin, A., Gnagne, T., N'Go, Y., Courivaud, J.-R. and co-authors. 2008. Caractérisation des sables et morphologie du fond du lac du barrage hydroélectrique de Taabo (Côte d'Ivoire). *Sci. Nat.* ***4***, 93–103. v4i1.42134.

Kozlova, E. A. and Manning, A. C. 2009. Methodology and calibration for continuous measurements of biogeochemical trace gas and $O_2$ concentrations from a 300-m tall tower in central Siberia. *Atmos. Meas. Tech.* **2**, 205–220.. doi:10.5194/amt-2-205-2009

Lacaux, J. P., Brustet, J. M., Delmas, R., Menaut, J. C., Abbadie, L. and co-authors. 1995. Biomass burning in the tropical savannas of Ivory Coast: An overview of the field experiment Fire of Savannas (FOS/DECAFE 91). *J. Atmos. Chem.* **22**, 195–216. doi:10.1007/BF00708189

Langenfelds, R. L., Francey, R. J., Pak, B. C., Steele, L. P., Lloyd, J. and co-authors. 2002. Interannual growth rate variations of atmospheric $CO_2$ and its $\delta^{13}C$, $H_2$, $CH_4$, and CO between 1992 and 1999 linked to biomass burning: Multispecies interannual variability. *Global Biogeochem. Cycles* **16**, 21–1–1048.

Levin, I., Ciais, P., Langenfelds, R., Schmidt, M., Ramonet, M. and co-authors. 2002. Three years of trace gas observations over the EuroSiberian domain derived from aircraft sampling — A concerted action. *Tellus B: Chem. Phys. Meteorol.* **54**, 696–712.

Liebmann, B., Dole, R. M., Jones, C., Bladé, I. and Allured, D. 2010. Influence of choice of time period on global surface temperature trend estimates. *Bull. Am. Meteor. Soc.* **91**, 1485–1492. doi:10.1175/2010BAMS3030.1

Lin, X., Indira, N. K., Ramonet, M., Delmotte, M., Ciais, P. and co-authors. 2015. Long-lived atmospheric trace gases measurements in flask samples from three stations in India. *Atmos. Chem. Phys.* **15**, 9819–9849. doi:10.5194/acp-15-9819-2015

Mahalakshmi, D. V., Badarinath, K. V. S. and Naidu, C. V. 2011. Influence of boundary layer dynamics on pollutant concentrations over urban region – A study using ground

based measurements. *Indian J. Radio Space Phys.* **40**, 147–152.

Mai, B., Deng, X., Zhang, F., He, H., Luan, T. and co-authors. 2020. Background characteristics of atmospheric $CO_2$ and the potential source regions in the Pearl River Delta Region of China. *Adv. Atmos. Sci.* **37**, 557–568. doi:10.1007/s00376-020-9238-z

Marnas, F. 2009. Mesure du dioxyde de carbone ($CO_2$) atmosphérique par Lidar Dial : Préparation d'une future mission spatiale. Thèse de doctorat. Institut Pierre-Simon Laplace (IPSL)/Laboratoire de Météorologie Dynamique (LMD), Paris, pp. 199.

McNorton, J., Chipperfield, M. P., Gloor, M., Wilson, C., Feng, W. and co-authors. 2016. Role of OH variability in the stalling of the global atmospheric $CH_4$ growth rate from 1999 to 2006. *Atmos. Chem. Phys.* **16**, 7943–7956. doi:10.5194/acp-16-7943-2016

Merbold, L., Ardö, J., Arneth, A., Scholes, R. J., Nouvellon, Y. and co-authors. 2009. Precipitation as driver of carbon fluxes in 11 African ecosystems. *Biogeosciences* **6**, 1027–1041. doi:10.5194/bg-6-1027-2009

Mikaloff Fletcher, S. E., Tans, P. P., Bruhwiler, L. M., Miller, J. B. and Heimann, M. 2004. $CH_4$ sources estimated from atmospheric observations of $CH_4$ and its $^{13}C/^{12}C$ isotopic ratios: 2. Inverse modeling of $CH_4$ fluxes from geographical regions. *Global Biogeochem. Cycles* **18,** 1–15.

Murayama, S., Saigusa, N., Chan, D., Yamamoto, S., Kondo, H. and co-authors. 2003. Temporal variations of atmospheric $CO_2$ concentration in a temperate deciduous forest in central Japan. *Tellus B: Chem. Phys. Meteorol.* **55**, 232–243. doi:10.3402/tellusb.v55i2.16751

Nacro, H. B. 2003. Le feu de brousse, un facteur de reproduction des écosystèmes de savanes à dominance herbacées à Lamto (Côte d'Ivoire)? *Rev. CAMES-Sér. A* **2**, 49–54.

N'dri, A. B., Fongbe, M., Soro, T. D., Gignoux, J., Kone, M. and co-authors. 2018. Principaux indices de l'intensité du feu dans une savane Guinéenne d'Afrique de l'Ouest. *Int. J. Bio. Chem. Sci.* **12**, 266–270. v12i1.21. doi:10.4314/ijbcs.v12i1.21

Niasse, M. 2004. Prévenir les conflits et promouvoir la coopération dans la gestion des fleuves transfrontaliers en Afrique de l'Ouest. Vertigo ***5****, 1–22*.

Pak, B. C. 2000. *Vertical Structure of Atmospheric Trace Gases over South-East Australia*. University of Melbourne, Melbourne, Victoria, Australia.

Pak, B. C. 2000. Vertical structure of atmospheric trace gases over South-east Australia, Ph.D. thesis. University of Melbourne, Melbourne, Victoria, Australia, pp. 273.

Palmer, P. I., Feng, L., Baker, D., Chevallier, F., Bösch, H. and co-authors. 2019. Net carbon emissions from African biosphere dominate pan-tropical atmospheric $CO_2$ signal. *Nat. Commun.* **10**, 3344. doi:10.1038/s41467-019-11097-w

Paris, J.-D., Stohl, A., Ciais, P., Nédélec, P., Belan, B. D. and co-authors. 2010. Source-receptor relationships for airborne measurements of $CO_2$, CO and $O_3$ above Siberia: a cluster-based approach. *Atmos. Chem. Phys.* **10**, 1671–1687. doi:10.5194/acp-10-1671-2010

Patra, P. K., Maksyutov, S. and Nakazawa, T. 2005. Analysis of atmospheric $CO_2$ growth rates at Mauna Loa using $CO_2$ fluxes derived from an inverse model. *Tellus B Chem. Phys. Meteorol.* **57**, 357–365. v57i5.16560. doi:10.3402/tellusb.v57i5.16560

Pedruzo-Bagazgoitia, X., de Roode, S. R., Adler, B., Babić, K., Dione, C. and co-authors. 2020. The diurnal stratocumulus-to-cumulus transition over land in southern West Africa. *Atmos. Chem. Phys.* **20**, 2735–2754. doi:10.5194/acp-20-2735-2020

Putaud, J. P., Arriga, N., Bergamaschi, P., Cavalli, F., Connoly, R. and co-authors. 2019. *The European Commission Atmospheric Observatory: 2018 Report*, EUR 30019EN, Publications Office of the European Union, Luxembourg. ISBN 978-92-76-14183-9. JRC118992.

Ramonet, M., Ciais, P., Nepomniachii, I., Sidorov, K., Neubert, R. E. M. and co-authors. 2002. Three years of aircraft-based trace gas measurements over the Fyodorovskoye southern taiga forest, 300 km north-west of Moscow. *Tellus B: Chem. Phys. Meteorol.* **54**, 713–734. v54i5.16720. doi:10.3402/tellusb.v54i5.16720

Rella, C. W., Chen, H., Andrews, A. E., Filges, A., Gerbig, C. and co-authors. 2013. High accuracy measurements of dry mole fractions of carbon dioxide and methane in humid air. *Atmos. Meas. Tech.* **6**, 837–860. doi:10.5194/amt-6-837-2013

Ringard, J., Dieppois, B., Rome, S., Dje Kouakou, B., Konaté, D. and co-authors. 2014. Évolution des pics de températures en Afrique de l'Ouest : étude comparative entre Abidjan et Niamey. Système et Interactions XXVIIe Colloque de l'Association International de Climatologie, Dijon, France, pp. 1–6.

Satar, E., Berhanu, T. A., Brunner, D., Henne, S. and Leuenberger, M. 2016. Continuous $CO_2$/CH4/CO measurements (2012–2014) at Beromünster tall tower station in Switzerland. *Biogeosciences* **13**, 2623–2635. doi:10.5194/bg-13-2623-2016

Scholes, R., Archibald, S. and von Maltitz, G. 2011. Emissions from fire in sub-saharan Africa: the magnitude of sources, their variability and uncertainty. Global Environ. Res. ***15***, 53–63.

Sreenivas, G., Mahesh, P., Subin, J., Kanchana, A. L., Rao, P. V. N. and co-authors. 2016. Influence of Meteorology and interrelationship with greenhouse gases ($CO_2$ and $CH_4$) at a suburban site of India. *Atmos. Chem. Phys.* **16**, 3953–3967. doi:10.5194/acp-16-3953-2016

Stein, A. F., Draxler, R. R., Rolph, G. D., Stunder, B. J. B., Cohen, M. D. and co-authors. 2015. NOAA's HYSPLIT atmospheric transport and dispersion modeling system. *Bull. Am. Meteor. Soc.* **96**, 2059–2077. doi:10.1175/BAMS-D-14-00110.1

Stohl, A., Forster, C., Frank, A., Seibert, P. and Wotawa, G. 2005. Technical note: The Lagrangian particle dispersion model FLEXPART version 6.2. *Atmos. Chem. Phys.* **5**, 2461–2474. doi:10.5194/acp-5-2461-2005

Stohl, A., Hittenberger, M. and Wotawa, G. 1998. Validation of the Lagrangian particle dispersion model FLEXPART against

large-scale tracer experiment data. *Atmos. Environ.* **32**, 4245–4264. doi:10.1016/S1352-2310(98)00184-8

Suntharalingam, P. 2004. Improved quantification of Chinese carbon fluxes using $CO_2$/CO correlations in Asian outflow. *J. Geophys. Res.* **109**, 1–13.

Ta, S., Kouadio, K. Y., Ali, K. E., Toualy, E., Aman, A. and co-authors. 2016. West Africa extreme rainfall events and large-scale ocean surface and atmospheric conditions in the tropical Atlantic. *Adv. Meteorol.* **2016**, 1–14. doi:10.1155/2016/1940456

Thoning, K. W., Tans, P. P. and Komhyr, W. D. 1989. Atmospheric carbon dioxide at Mauna Loa Observatory: 2. Analysis of the NOAA GMCC data, 1974-1985. *J. Geophys. Res.* **94**, 8549–8565. doi:10.1029/JD094iD06p08549

Tiemoko, D. T., Yoroba, F., Diawara, A., Kouadio, K., Kouassi, B. K. and co-authors. 2020a. Understanding the local carbon fluxes variations and their relationship to climate conditions in a sub-humid savanna-ecosystem during 2008-2015: Case of Lamto in Côte d'Ivoire. *ACS.* **10**, 186–205. doi:10.4236/acs.2020.102010

Tiemoko, D. T., Yoroba, F., Paris, J.-D., Diawara, A., Berchet, A. and co-authors. 2020b. Source–receptor relationships and cluster analysis of $CO_2$, $CH_4$, and CO concentrations in West Africa: The case of Lamto in Côte d'Ivoire. *Atmosphere* **11**, 903. doi:10.3390/atmos11090903

Tohjima, Y., Kubo, M., Minejima, C., Mukai, H., Tanimoto, H. and co-authors. 2014. Temporal changes in the emissions of $CH_4$ and CO from China estimated from $CH_4$/$CO_2$ and CO/$CO_2$ correlations observed at Hateruma Island. *Atmos. Chem. Phys.* **14**, 1663–1677. doi:10.5194/acp-14-1663-2014

Touré, N. E., Konaré, A. and Silué, S. 2012. Intercontinental transport and climatic impact of Saharan and Sahelian dust. *Adv. Meteorol.* **2012**, 1–14. doi:10.1155/2012/157020

Turnbull, J. C., Miller, J. B., Lehman, S. J., Tans, P. P., Sparks, R. J. and co-authors. 2006. Comparison of $14CO_2$, CO, and $SF_6$ as tracers for recently added fossil fuel $CO_2$ in the atmosphere and implications for biological $CO_2$ exchange. *Geophys. Res. Lett.* **33**, n/a–n/a. n/a-n/a. doi:10.1029/2005GL024213

UNDP. 2015. World population prospects: The 2012 revision. http://esa.un.org/unpp.

Wada, A., Matsueda, H., Sawa, Y., Tsuboi, K. and Okubo, S. 2011. Seasonal variation of enhancement ratios of trace gases observed over 10 years in the western North Pacific. *Atmos. Environ.* **45**, 2129–2137. doi:10.1016/j.atmosenv.2011.01.043

Wang, G., Huang, J., Guo, W., Zuo, J., Wang, J. and co-authors. 2010. Observation analysis of land-atmosphere interactions over the Loess Plateau of northwest China. *J. Geophys. Res.* **115**, 1–15.

Ward, D. E., Sandberg, D. V., Ottmar, R. D., Frost, J. A., Hofner, G. G., and Fitzsimmons, C. K. 1982. *Measurements of Smokes from Two Prescribed Fires in the Pacific Northwest, Seventy-Fifth Annual Meeting of the Air Pollution Control Association* (Ward, D. E., ed.). USDA Forest Service, Intermountain Fire Science Laboratory, Missoula, Montana, pp. 59807.

van der Werf, G. R., Randerson, J. T., Giglio, L., Collatz, G. J., Mu, M. and co-authors. 2010. Global fire emissions and the contribution of deforestation, savanna, forest, agricultural, and peat fires (1997–2009). *Atmos. Chem. Phys.* **10**, 11707–11735. doi:10.5194/acp-10-11707-2010

WMO. 2017. Greenhouse Gases and Other Atmospheric Gases, World Data Centre for Greenhouse Gases (WDCGG) Data Summary, WDCGG No. 41, pp. 99. https://gaw.kishou.go.jp/static/publications/summary/sum41/sum41.pdf

Wong, K. W., Fu, D., Pongetti, T. J., Newman, S., Kort, E. A. and co-authors. 2014. Mapping $CH_4$: $CO_2$ ratios in Los Angeles with CLARS-FTS from Mount Wilson, California. *Atmos. Chem. Phys. Discuss.* **14**, 17037–17066. doi:10.5194/acpd-14-17037-2014

Wu, C. and Yu, J. Z. 2018. Evaluation of linear regression techniques for atmospheric applications: the importance of appropriate weighting. *Atmos. Meas. Tech.* **11**, 1233–1250. doi:10.5194/amt-11-1233-2018

Xia, L., Zhang, G., Zhan, M., Li, B. and Kong, P. 2020. Seasonal variations of atmospheric CH4 at Jingdezhen station in Central China: Understanding the regional transport and its correlation with $CO_2$ and CO. *Atmos. Res.* **241**, 104982. doi:10.1016/j.atmosres.2020.104982

Xiao, Y. 2004. Constraints on Asian and European sources of methane from CH4 -C2H6 -CO correlations in Asian outflow. *J. Geophys. Res.* **109**, D15S16.

Yokelson, R. J., Susott, R., Ward, D. E., Reardon, J. and Griffith, D. W. T. 1997. Emissions from smoldering combustion of biomass measured by open-path Fourier transform infrared spectroscopy. *J. Geophys. Res.* **102**, 18865–18877. doi:10.1029/97JD00852

Yver Kwok, C., Laurent, O., Guemri, A., Philippon, C., Wastine, B. and co-authors. 2015. Comprehensive laboratory and field testing of cavity ring-down spectroscopy analyzers measuring $H_2O$, $CO_2$, $CH_4$ and CO. *Atmos. Meas. Tech.* **8**, 3867–3892.

## Appendice

*Table A1.* List of the three calibration scales used at Lamto between 2008 and 2020.

| ID | Type | Start | CO2 | *Inst* | Scale | CH4 | *Inst* | Scale | CO | *Inst* | Scale |
|---|---|---|---|---|---|---|---|---|---|---|---|
| D481347 | Luxfer_Alu_B10 | 27/08/2008 | **339.34** | *Loflo2D* | WMO.X2007 | **1737.1** | *GC-HP.2* | WMO X2004A | – | – | – |
| D481355 | Luxfer_Alu_B10 | 27/08/2008 | **374.66** | *Loflo2D* | WMO.X2007 | **1837.0** | *GC-HP.2* | WMO X2004A | – | – | – |
| D481323 | Luxfer_Alu_B10 | 27/08/2008 | **401.90** | *Loflo2D* | WMO.X2007 | **2030.8** | *GC-HP.2* | WMO X2004A | – | – | – |
| D481341 | Luxfer_Alu_B10 | 27/08/2008 | **463.88** | *Loflo2D* | WMO.X2007 | **2223.4** | *GC-HP.2* | WMO X2004A | – | – | – |
| D609151 | Luxfer_Alu_B40 | 26/10/2010 | **351.46** | *CRDS-G2401.119* | WMO.X2007 | **1765.3** | *CRDS-G2401.119* | WMO X2004A | – | – | – |
| D609137 | Luxfer_Alu_B40 | 26/10/2010 | **380.80** | *CRDS-G2401.119* | WMO.X2007 | **1856.3** | *CRDS-G2401.119* | WMO X2004A | – | – | – |
| D609146 | Luxfer_Alu_B40 | 26/10/2010 | **410.88** | *CRDS-G2401.119* | WMO.X2007 | **1979.8** | *CRDS-G2401.119* | WMO X2004A | – | – | – |
| D609135 | Luxfer_Alu_B40 | 26/10/2010 | **462.55** | *CRDS-G2401.119* | WMO.X2007 | **2111.0** | *CRDS-G2401.119* | WMO X2004A | – | – | – |
| D141320 | Luxfer_Alu_B40 | 31/03/2014 | **370.33** | *CRDS-G2401.119* | WMO.X2007 | **1812.1** | *CRDS-G2401.119* | WMO X2004A | **114.6** | *CRDS-G2401.119* | WMO.CO.X2014A |
| D141324 | Luxfer_Alu_B40 | 31/03/2014 | **390.16** | *CRDS-G2401.119* | WMO.X2007 | **1958.7** | *CRDS-G2401.119* | WMO X2004A | **179.1** | *CRDS-G2401.119* | WMO.CO.X2014A |
| D141325 | Luxfer_Alu_B40 | 31/03/2014 | **410.72** | *CRDS-G2401.119* | WMO.X2007 | **2005.6** | *CRDS-G2401.119* | WMO X2004A | **208.7** | *CRDS-G2401.119* | WMO.CO.X2014A |
| D141330 | Luxfer_Alu_B40 | 31/03/2014 | **450.69** | *CRDS-G2401.119* | WMO.X2007 | **2304.1** | *CRDS-G2401.119* | WMO X2004A | **259.1** | *CRDS-G2401.119* | WMO.CO.X2014A |

Each scale is made of four cylinders whose concentrations were spanning atmospheric range. The LSCE instruments used to assign the values of each cylinder are indicated in the columns entitled 'Inst'.

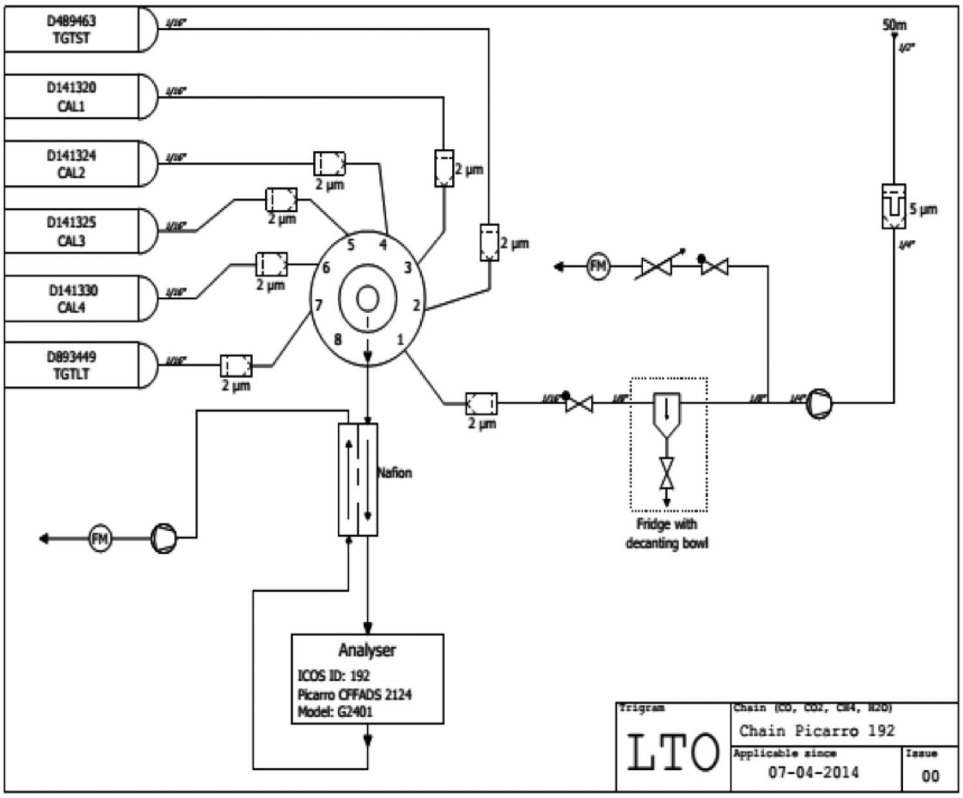


Fig. A1. Schematic diagram of the air sampling analysis line for the measurement of $CO_2$, $CH_4$ and CO concentrations by "PICARRO" at Lamto.